nature portfolio

Peer Review File

Solar and thermal dual-band electrochromic windows for energy-efficient buildings

Corresponding Author: Professor Jia Zhu

This file contains all reviewer reports in order by version, followed by all author rebuttals in order by version.

Version 0:

Reviewer comments:

Reviewer #1

(Remarks to the Author)
This manuscript presents a Cu–Bi-based RME (Reversible Metal Electrodeposition) system integrated into a spatially dynamic architecture for a dual-mode electrochromic window. The results demonstrate significant advantages in energy savings and combined solar/thermal regulation. However, I have several specific points that should be addressed to enhance clarity and reproducibility for readers.
1. Supplementary Fig. 17 reports depositing/stripping times of 13.8 s and 6.6 s, respectively, while Supplementary Fig. 20 shows a coloring process taking roughly 50 s for a 2.5 cm × 2.5 cm sample. Please clarify what experimental criteria or conditions (e.g., cell size, current density, electrode distance, measurement protocols, or readout methods) account for the significant difference in switching times between these figures. Are these results directly comparable? If not, please identify the main variable(s) contributing to this difference.
2. Supplementary Fig. 20 does not provide a visual sequence for the bleaching (decoloration) process. Under the same experimental conditions as those used in the coloring test, what is the actual time required for the window to fully return to a transparent state, as observed visually? Please provide quantitative details and clarify your “bleaching complete” criterion.
3. The manuscript would benefit from additional clarification on the ion-transport mechanism at the electrode–electrolyte interface. Specifically, how is the Cu–Bi film formed and subsequently removed under the applied bias and cycling conditions? Please link this mechanism to the current-time features observed in Supplementary Fig. 19, including any discussion of nucleation, growth, or dissolution processes, and how they affect switching speed, reversibility, and cycle stability.
4. While Fig. 2g demonstrates that the deposited (colored) state remains stable for 36 hours under open-circuit conditions, the stability/retention time of the transparent state is not reported. Please provide quantitative data for how long the transparent state is maintained under open-circuit conditions, and clarify the practical/experimental procedure followed for the stripping process.
5. Is it possible to achieve additional coloration states or hues by modifying the electrolyte composition or pH, or through structural changes to the device? Can the electrolyte thickness be controlled systematically, and if so, how does this influence switching performance, including speed, efficiency, or color contrast?
6. In the vertical thermal cycling test, normal glass and low-E glass show pronounced temperature fluctuations, while STDEC and EC samples do not. Please clarify which physical or material properties of the STDEC/EC windows are responsible for this effect—e.g., thermal insulation, emissivity, or other factors.

Reviewer #2

(Remarks to the Author)
The manuscript reports a solar and thermal dual-band electrochromic smart window capable of modulating both solar transmission and long-wave infrared emissivity, thereby enabling all-season control of building energy. The approach integrates a reversible metal electrodeposition electrochromic system with a mechanical rotation mechanism to independently control solar transmittance and thermal emissivity. The concept is novel and significant in the field of smart windows. The approach is both conceptually innovative and practically impactful. While I would be happy to recommend it for publication, there are a few concerns that need to be addressed to further improve the manuscript.
While the RME cycling stability is well documented for 2000 cycles, the long-term performance under environmental stress remains insufficiently addressed. How does the electrolyte hold up under extended UV exposure, weathering, or temperature/humidity cycling?

The soft PE layer on the front side might be fragile to wind/rain/snow/etc. In this work, an outdoor experiment was conducted at very low wind speeds, with an average of 2 m/s. How to protect this device from heavy rain/snow, or strong winds/dust? The aqueous PVA-based electrolyte might be prone to drying out or freezing in cold climates. Can the authors comment on the layer adhesion and electrode contact in relation to thermal stress between high-heat-gain and deep-cooling cycling states? Also, the electrolyte system is highly corrosive and toxic; does the electrolyte leach out during the same thermal stress?
Is the STDEC window view distortion-free? Also, the study doesn't mention haze or clarity. The authors should address this. The building energy-saving simulation indicates an annual HVAC energy savings of up to 80 MJ/m² in extreme climate zones. Did the simulation account for the manufacturing costs, service life, and maintenance costs of the STDEC windows? In addition, the solar heat gain coefficient is an important parameter to evaluate a window, especially for an EC window. However, such fundamental data on the STDEC device is missing. Additionally, the energy simulations appear to assume an identical U-value for all window configurations; The authors should address this.
While the optimized ITO layer of 185nm is needed, scaling the RME system to meter-scale architectural windows presents challenges regarding uniformity and switching kinetics. The authors should comment on how to maintain the same performance of a 100 cm² device across larger dimensions, typical of commercial windows.

Version 1:

Reviewer comments:

Reviewer #1

(Remarks to the Author)
Now, there are no concerns. I recommend to accept this paper.

Reviewer #2

(Remarks to the Author)
I am impressed by both the quantity and the quality of the work carried out on the manuscript during the revision process. The authors addressed the extensive comments from all reviewers. Results are very solid and clearly presented. The overall quality of the paper has significantly improved. I recommend acceptance in its present form.

Response to Referee Reports for "Solar and Thermal Dual-Band Electrochromic Windows for Energy-Efficient Buildings"

We sincerely thank all reviewers for their timely review, constructive feedback, and positive assessment of our work. Guided by these valuable suggestions, we have strengthened the manuscript through additional experiments, expanded analyses, and deeper discussions.

Key revisions include:

1. Electrochromic performance metrics. The electrochromic coloration/bleaching times were distinguished from the depositing/stripping times due to differences in measurement protocols and device sizes. Furthermore, a transparent-state stability time of 36 hours and low haze values of <1% were demonstrated, highlighting the excellent bistability and optical clarity of the STDEC window.

2. Electrodeposition mechanism of the Cu–Bi film. The formation and removal mechanism of the Cu–Bi film under bias and cycling conditions was elucidated, confirming the critical role of Cu^{2+} in nucleation, growth, and dissolution, and thus enhancing the switching speed, reversibility, and cycling stability of Cu–Bi deposition system compared with a Bi-only deposition system.

3. Window stability. The STDEC windows were subjected to rigorous durability tests, including extended UV exposure, weathering, temperature/humidity cycling, and extreme high and low temperatures, confirming excellent stability.

4. Building energy saving simulation. The results of building energy saving simulation were updated to incorporate the measured *U*-values and a techno-economic assessment (TEA) analysis.

Together, these revisions substantially improve the clarity, rigor, and completeness of the manuscript and further strengthen the scientific and technological contributions of our study.

Please find below our point-by-point responses to all reviewers' comments, with revisions indicated where appropriate. The line, figure, and page numbers refer to the revised manuscript and revised supplementary materials.

This document uses the following convention:

1. Blue—original reviewer's reports
2. Black—our response to the comments
3. Red—additions/changes made to the manuscript

Response to Reviewer 1

[General Comment]: This manuscript presents a Cu–Bi-based RME (Reversible Metal Electrodeposition) system integrated into a spatially dynamic architecture for a dual-mode electrochromic window. The results demonstrate significant advantages in energy savings and combined solar/thermal regulation. However, I have several specific points that should be addressed to enhance clarity and reproducibility for readers.

[Response]: We are grateful to Reviewer 1 for the valuable comments. All the issues raised have been meticulously examined and addressed point by point, as detailed below, to enhance the clarity and reproducibility of the manuscript.

[Comment 1]: Supplementary Fig. 17 reports depositing/stripping times of 13.8 s and 6.6 s, respectively, while Supplementary Fig. 20 shows a coloring process taking roughly 50 s for a 2.5 cm × 2.5 cm sample. Please clarify what experimental criteria or conditions (e.g., cell size, current density, electrode distance, measurement protocols, or readout methods) account for the significant difference in switching times between these figures. Are these results directly comparable? If not, please identify the main variable(s) contributing to this difference.

[Response]: We thank the reviewer for this insightful comment regarding the switching times. We would like to clarify that the significant difference in switching times between Supplementary Fig. 17 and Supplementary Fig. 20 is primarily due to differences in measurement protocols and device sizes.

(i) Measurement protocol

Figure R1 presents the electrochromic switching times (13.8 s and 6.6 s) obtained using the standard measurement method under constant voltage condition, specifically a coloration time of 13.8 s for Cu–Bi depositing and a bleaching time of 6.6 s for Cu–Bi stripping, respectively. In this method, the optical response is monitored in real time, and the switching time is typically defined as the duration required for the transmittance or absorbance change at a specific wavelength to reach 90% of the total variation under a step voltage. This approach focuses on the intrinsic response speed of the electrochromic material. To avoid any confusion with depositing/stripping times shown in **Figure R2**, the term “switching time” in this manuscript refers to the electrochromic coloration/bleaching time.

In contrast, **Figure R2** shows the depositing/stripping times during the coloration/bleaching processes under constant voltage conditions. When a constant voltage of +1V is applied, the device requires roughly 50 s to change from the transparent bleached state to a steady colored state. Conversely, when an opposite constant voltage of –1 V is applied, the device takes about 20 s to fully return from the black colored state to a steady bleached state. These times are not strictly "response times", but rather represent the total times of applied voltages required for the coloration and bleaching states to stabilize.

(ii) Device size

The device used in **Figure R1** has an active area of about 10 cm^2 (3 cm × 3 cm), whereas the sample in **Figure R2** is larger**,** measuring 25 cm^2 (5 cm × 5 cm). Larger-area devices typically exhibit higher voltage drops and less uniform electric field distribution, leading to significantly longer overall switching times.

Therefore, these results are not directly comparable as they highlight different performance aspects, with the differences stemming from variations in measurement protocols and device sizes.

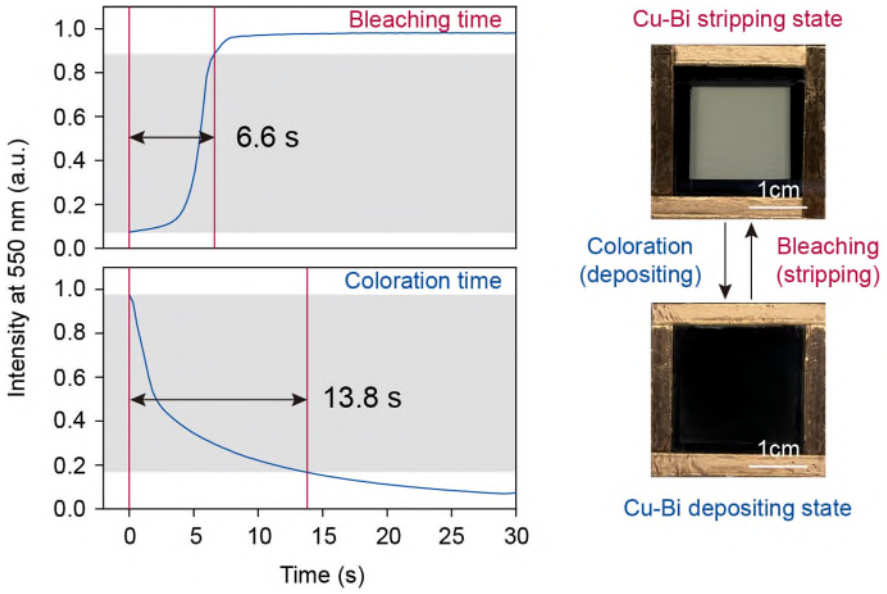

Figure R1. The switching times were derived from normalized transmission spectra following the standard electrochromic measurement protocol. Defined as the time required for the transmittance change at a specific wavelength to reach 90% of its total variation in response to a step voltage, the switching times measured in experiments for the ~10 cm^2 STDEC window show a bleaching time of 6.6 s for Cu-Bi stripping and a coloration time of 13.8 s for Cu-Bi depositing.

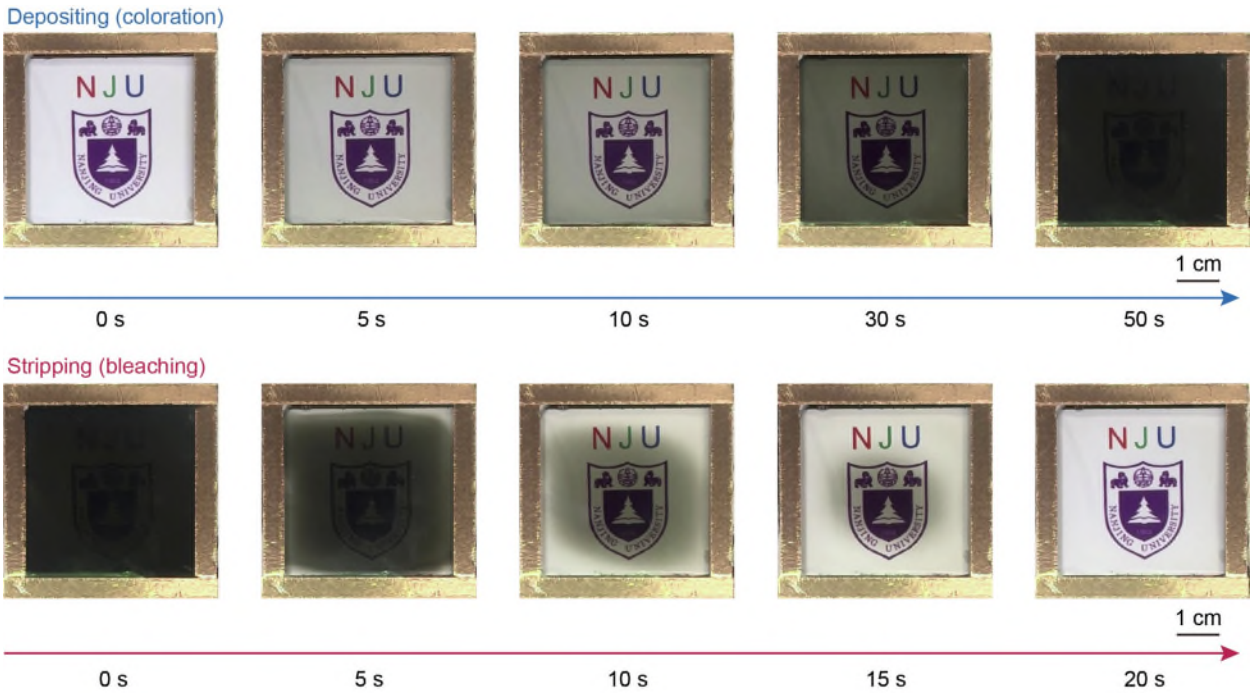

Figure R2. Optical photographs of the Cu-Bi film depositing (coloration) and stripping (bleaching) processes in a 25 cm^2 STDEC window.

[Changes in revised manuscript]:

We have made one main change in the revised manuscript and SI.

1. Page 11 of the revised manuscript.

We expanded the sentence and the figure caption to emphasize the measurement protocol and the device size used in the switching time measurement:

"*Furthermore, the switching time of a ~10 cm^2 STDEC window is evaluated to characterize the response speed of the Cu–Bi material by recording the transmittance intensity of clear and colored states at 550 nm using a fiber optic spectrometer, indicating a bleaching time of 6.6 s for Cu–Bi stripping and a coloration time of 13.8 s for Cu–Bi depositing (Supplementary Fig. 22).*

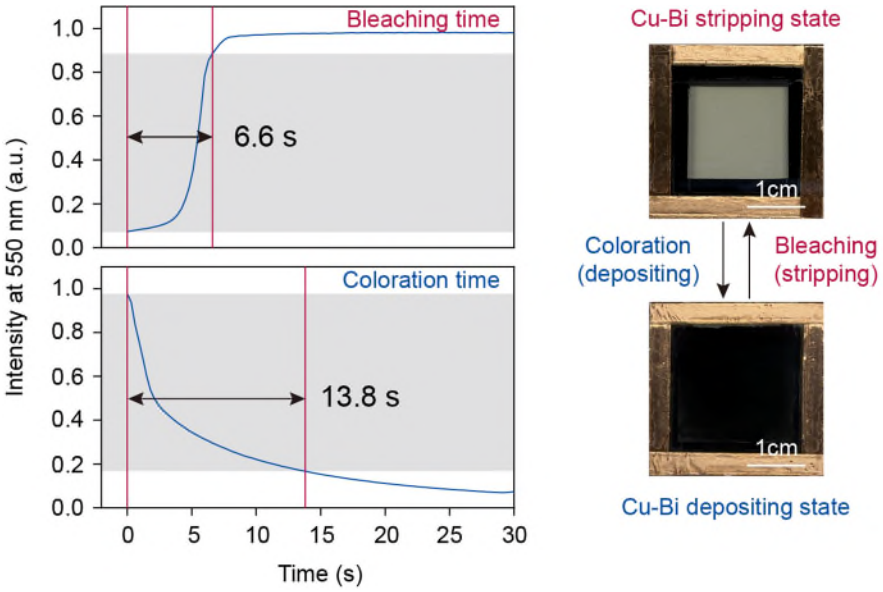

Supplementary Fig. 22: The switching times were derived from normalized transmission spectra following the standard electrochromic measurement protocol. Defined as the time required for the transmittance change at a specific wavelength to reach 90% of its total variation in response to a step voltage, the switching times measured in experiments for the ~10 cm^2 STDEC window show a bleaching time of 6.6 s for Cu–Bi stripping and a coloration time of 13.8 s for Cu–Bi depositing."

[Comment 2]: Supplementary Fig. 20 does not provide a visual sequence for the bleaching (decoloration) process. Under the same experimental conditions as those used in the coloring test, what is the actual time required for the window to fully return to a transparent state, as observed visually? Please provide quantitative details and clarify your "bleaching complete" criterion.

[Response]: We thank the reviewer for this constructive suggestion. **Figure R2** provides a visual sequence for the bleaching (decoloration) process. The depositing/stripping times are presented in response to the coloration/bleaching processes under the same experimental conditions. When a constant voltage of +1V is applied, the window requires about 50 s to change from the transparent bleached state to a steady colored state. When a reverse constant voltage of –1 V is applied, the window takes approximately 20 s to fully return from the black colored state to the transparent bleached state. Therefore, as observed visually, the actual time required for complete bleaching in a 25 cm^2 STDEC window is about **20 s**.

Our **"bleaching complete" criterion** is defined as the bleaching spectrum in the solar region returning exactly to the initial transparent state. As illustrated in **Figure R3**, the solar transmittance

in the bleached state ($T_{sol\text{-}bleach}$ = 52.4%) recovers to ~100% of its initial state value ($T_{sol\text{-}initial}$ = 52.2%), and the window appears fully transparent with no residual color upon visual inspection (**Figure R2**). At this point, the bleaching process is considered complete.

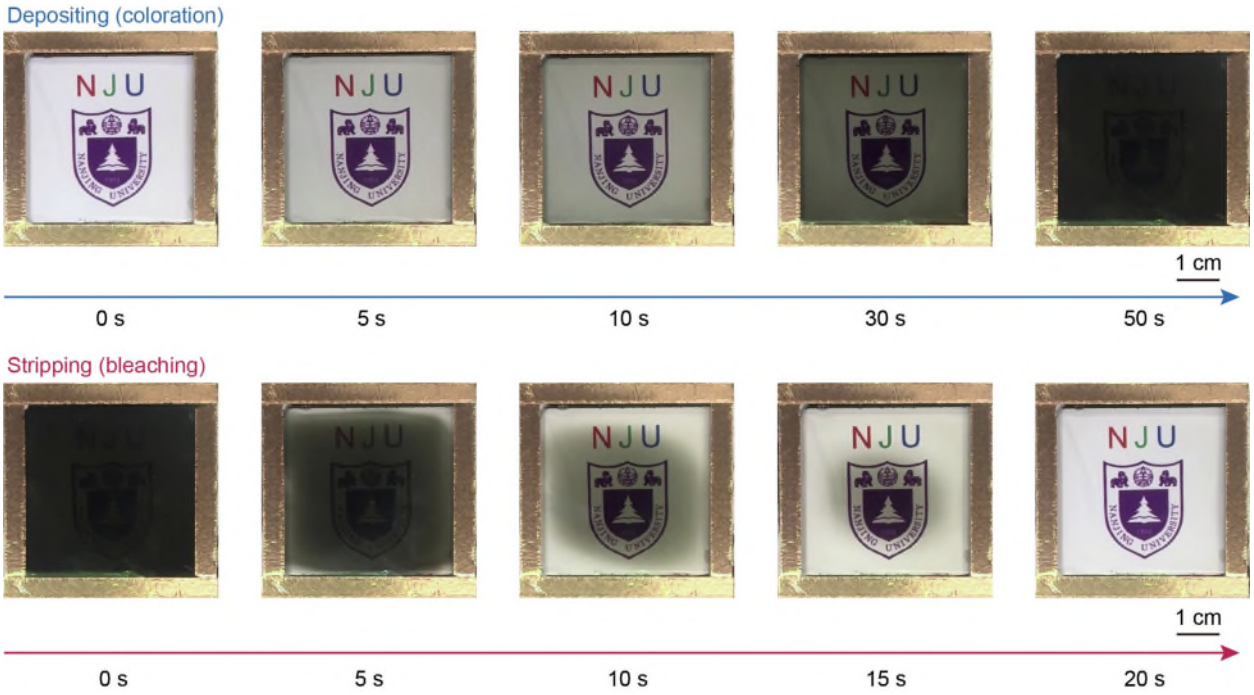

Figure R2. Optical photographs of the Cu–Bi film depositing (coloration) and stripping (bleaching) processes in a 25 cm^2 STDEC window.

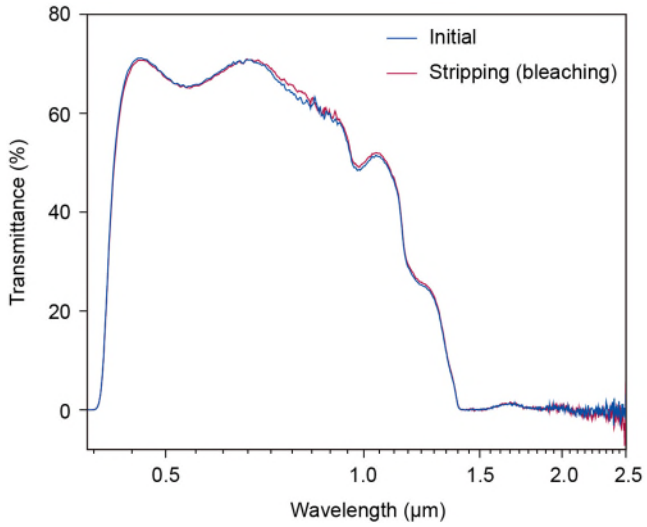

Figure R3. Transmittance spectra of the STDEC window in the solar range (0.38–2.5 μm) for both the initial and bleached states, respectively. The solar transmittance returns to its initial state value through the complete bleaching of the Cu–Bi film.

[Changes in revised manuscript]:

We have made two main changes in the revised manuscript and SI.

1. Page 6 of the revised manuscript.

We added the sentence to highlight the "bleaching complete" criterion:

"*This high T_{sol} can be cyclically restored through the complete bleaching of the RME film (Supplementary Fig. 8).*

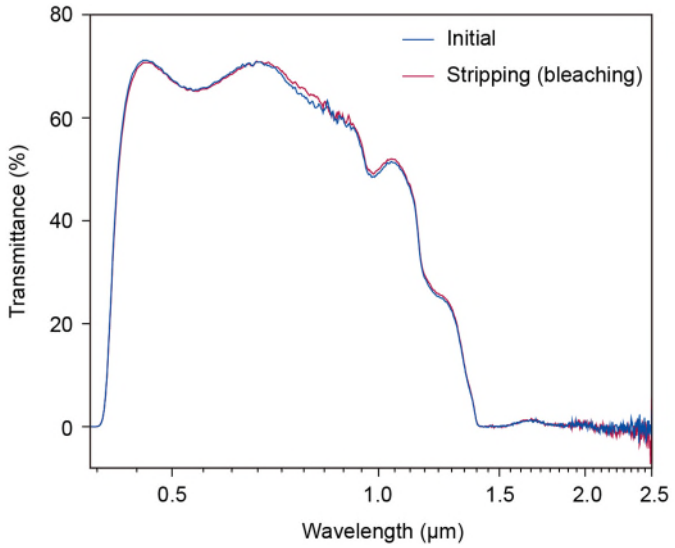

Supplementary Fig. 8: Transmittance spectra of the STDEC window in the solar range (0.38–2.5 μm) for both the initial and bleached states, respectively. The solar transmittance returns to its initial state value through the complete bleaching of the Cu–Bi film."

2. Page 12 of the revised manuscript.

We added a discussion to emphasize a visual sequence for the bleaching (decoloration) process:

"*Upon stripping, the L* color coordinate rises markedly, returning to its original level after complete bleaching, while the a* and b* projections remain centered (Supplementary Fig. 26 and Supplementary Table 5). This indicates a reverse neutral color transition from black back to initial transparent state.*

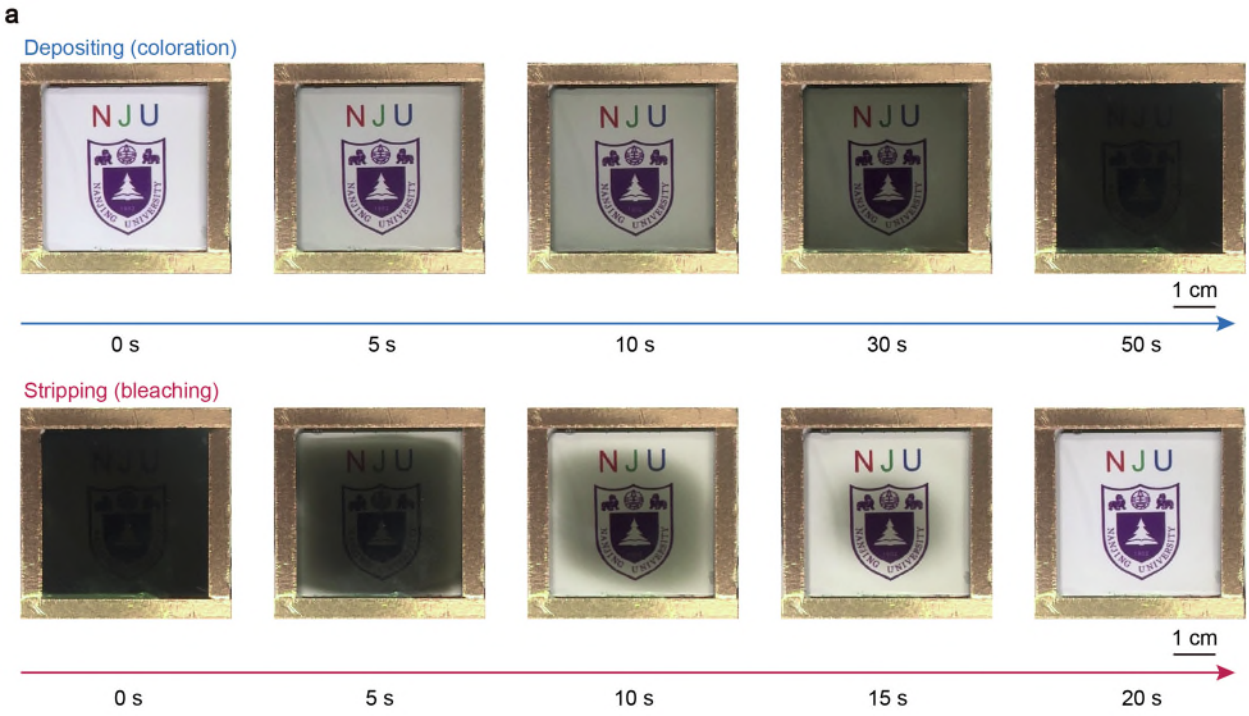
a
Depositing (coloration)
NJU
1 cm
0 s
5 s
10 s
30 s
50 s
Stripping (bleaching)
1 cm
0 s
5 s
10 s
15 s
20 s

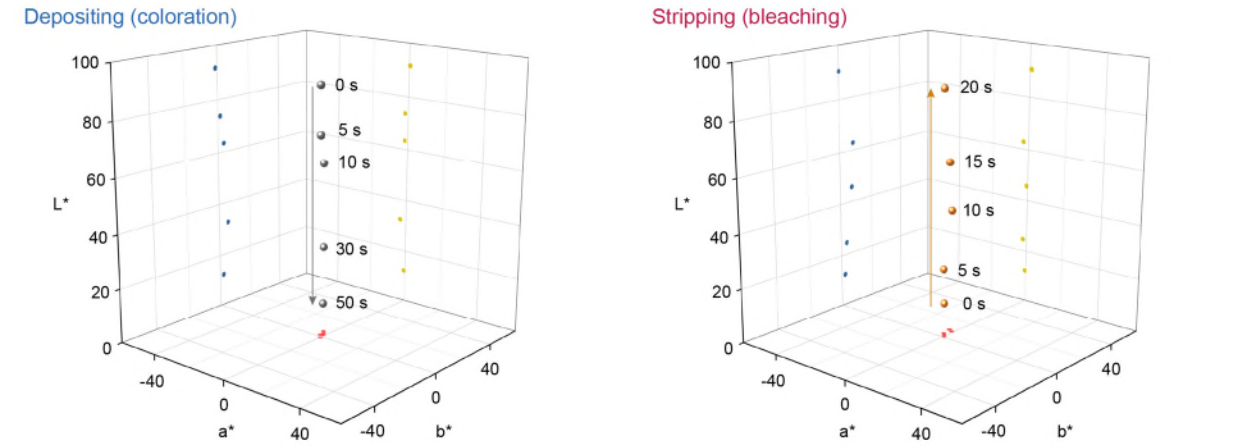
b
Depositing (coloration)
Stripping (bleaching)
L*
a*
b*
0 s
5 s
10 s
30 s
50 s
15 s
20 s

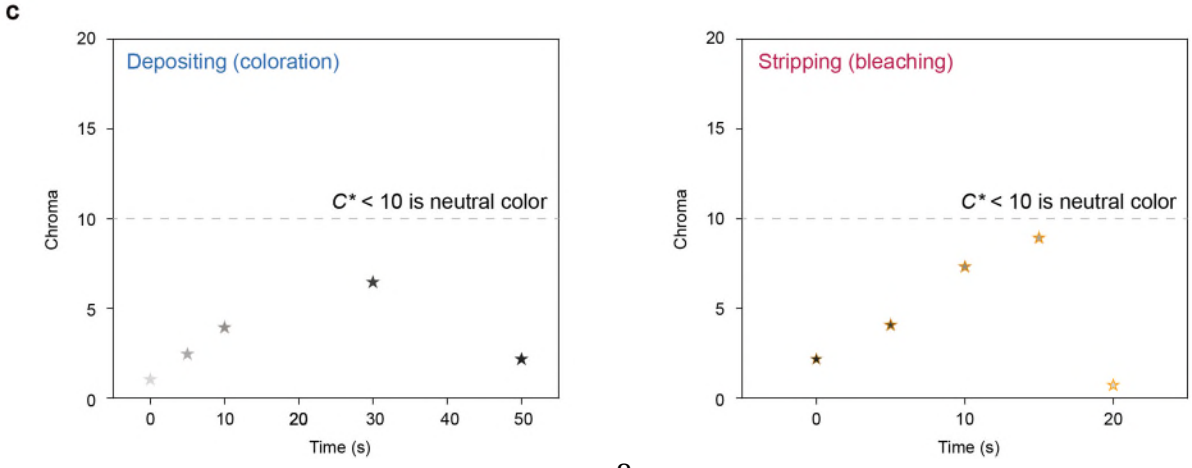
c
Depositing (coloration)
Stripping (bleaching)
Chroma
Time (s)
C* < 10 is neutral color

Supplementary Fig. 26: Color neutrality characterization of the STDEC window. **a**, Optical photographs of a 25 cm^2 STDEC window during the Cu–Bi depositing (coloration) and stripping (bleaching) processes, illustrating a neutral color transition (clear-to-grey-to-black) throughout the RME process. **b**, $L^*a^*b^*$ coordinates for various optical states at different depositing and stripping times. **c**, The color neutrality is characterized by the chroma (C^*) value in the CIE $L^*a^*b^*$ color space. If C^* is below 10, the STDEC window displays a neutral color across its full optical state range during the RME process.

Supplementary Table 5. $L^*a^*b^*$ and chroma (C^*) measurements of a STDEC window at various stripping times.

Stripping time (s)	L^*	a^*	b^*	C^*
0	12.1	-0.7	2.0	2.1
5	24.5	-2.2	3.4	4.0
10	45.7	-0.7	7.3	7.3
15	62.8	-3.0	8.4	8.9
20	90.4	0.7	0.2	0.7

Note: L^* quantifies lightness on a scale from 0 (black) to 100 (white), a^* indicates the green to red ranging from -128 (pure green) to +128 (pure red), and b^* measures the blue to yellow ranging from -128 (pure blue) to +128 (pure yellow). C^* is a metric that combines a^* and b^* values in the color space to characterize the overall color of the STDEC window. When C^* is less than 10, it becomes challenging for the human eye to differentiate the color of the window, leading to a perception of color neutrality. In these instances, the C^* value falls below 10 for STDEC window, resulting in a color-neutral appearance."

[Comment 3]: The manuscript would benefit from additional clarification on the ion-transport mechanism at the electrode–electrolyte interface. Specifically, how is the Cu–Bi film formed and subsequently removed under the applied bias and cycling conditions? Please link this mechanism to the current-time features observed in Supplementary Fig. 19, including any discussion of

nucleation, growth, or dissolution processes, and how they affect switching speed, reversibility, and cycle stability.

[Response]: We thank the reviewer for this constructive suggestion. We have elucidated the formation and removal mechanism of the Cu–Bi film under applied bias and cycling conditions, and directly linked these processes to the current–time features. We also discuss the nucleation, growth, and dissolution behaviours of Cu–Bi films and explain how they influence switching speed, reversibility, and cycling stability compared to a system with only Bi film deposition. The details are as follows:

(i) Formation and removal mechanism of the Cu–Bi film

Figure R4 shows the cyclic voltammetry (CV) curve for the deposition and stripping of the Cu–Bi film, obtained within a voltage range of –1.0 V to +1.0 V at 50 mV/s. During the initial negative-going sweep, the cathodic current starts to rise at 0.52 V, attributed to the reduction of Cu^{2+} to Cu^{+} without any metal deposition. A further increase in cathodic current at –0.2 V, corresponds to the reduction of Bi^{3+} to Bi and Cu^{+} to Cu. At this phase, Cu^{+} can participate in galvanic displacement reactions with dendritic Bi atoms and fill in void spaces with three times the number of Cu atoms, resulting in a more condensed spherical morphology that suppresses dendritic growth (**Figure R5**).

During the subsequent positive-going sweep, the negative current indicates the continued reduction of metal ions to Cu–Bi films deposited on the working electrode. Anodic current begins to increase at –0.1 V, due to the dissolution of the Cu and Bi back to Cu^{+} and Bi^{3+}, respectively. At this stage, Cu^{+} can also speed up the dissolution of Bi via galvanic displacement reactions, leaving no residual dead Bi (**Figure R5**). Cu^{+} is then further oxidized to Cu^{2+} at voltages more positive than 0.65 V.

These deposition and stripping processes can be linked to the current–time curve (**Figure R6**). When a negative voltage (–1.0 V) is applied, the current–time curve exhibits a transient current peak (**Figure R6**, **i**), indicating the instantaneous nucleation of Cu–Bi clusters on the electrode surface. After this peak, the current slowly decays and reaches a diffusion-controlled plateau phase (**Figure R6**, **ii**), reflecting the concurrent nucleation and growth of the Cu–Bi film. When the bias is reversed to +1.0 V, a reverse anodic current peak appears (**Figure R6**, **iii**) and then gradually diminishes (**Figure R6**, **iv**), which corresponds to the stripping and dissolution of the Cu–Bi film. These symmetric peaks, with a charge of about 100.5 mC/cm^2, indicate excellent electrochemical reversibility and stable cycling performance of the Cu–Bi film.

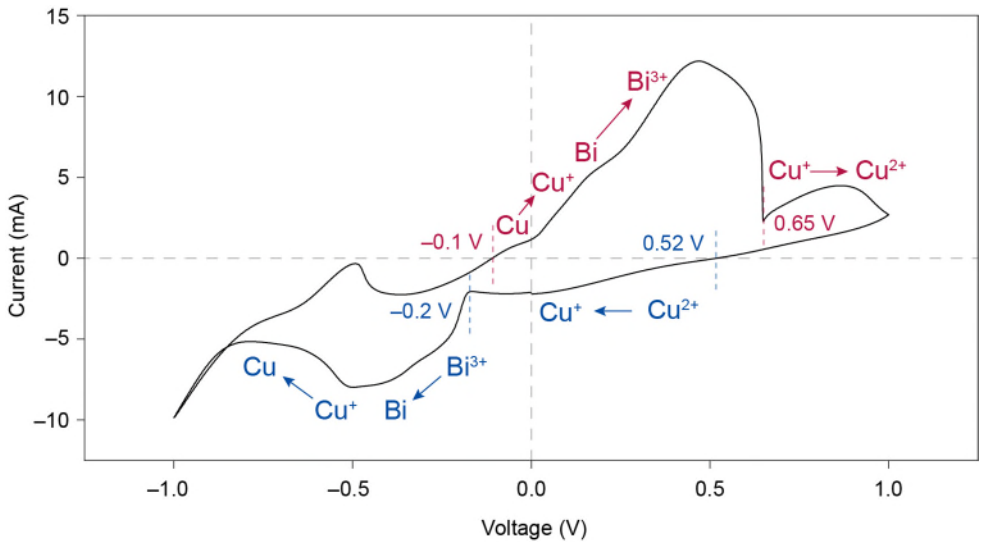

Figure R4. Cyclic voltammogram of the Cu–Bi film measured between –1.0 V and +1.0 V at 50 mV/s.

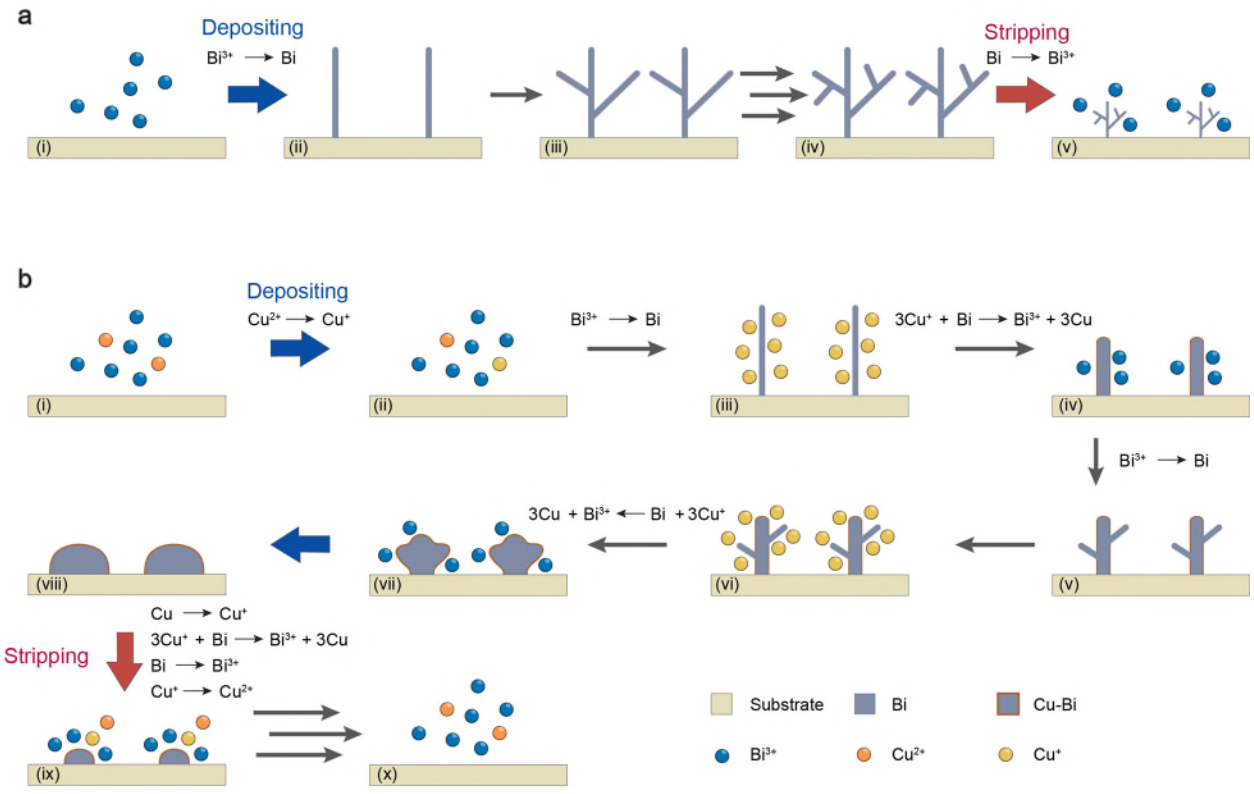

Figure R5. Reaction schematic for the deposition and stripping of Bi films in the (**a**) absence and (**b**) presence of Cu^{2+}.

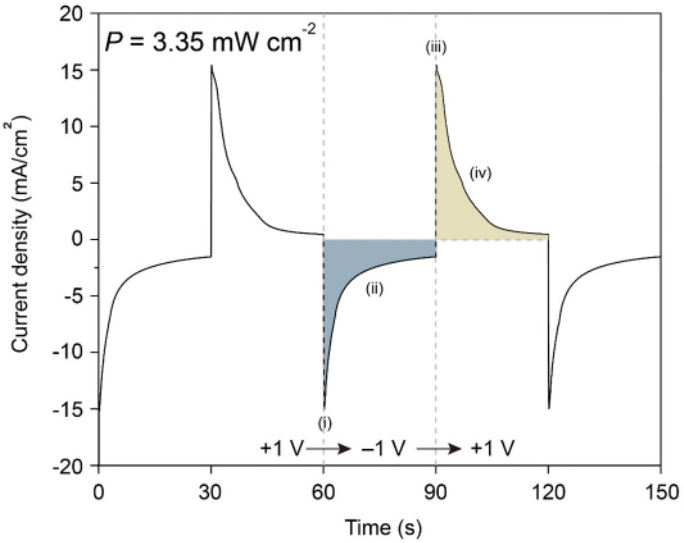

Figure R6. Chronoamperometric curve of the STDEC window. The current–time curve shows the distinct stages of the Cu–Bi film deposition and stripping: (i) instantaneous nucleation of Cu–Bi clusters; (ii) concurrent nucleation and growth; (iii, iv) stripping and dissolution of the Cu–Bi film. These symmetric peaks (charge ~100.5 mC/cm^2) indicate excellent electrochemical reversibility and stable cycling performance, with an average power consumption of 3.35 mW cm^{-2}.

(ii) Key effects of Cu^{2+} addition to the deposition and stripping of Cu–Bi films

Cu^{2+} critically governs the deposition and stripping of Cu–Bi films, determining switching speed, reversibility, and cycling stability. Upon deposition, Cu^{2+} is reduced to Cu^{+}, which drives galvanic displacement of Bi and promotes the nucleation and growth of spherical particles. Upon stripping, Cu is oxidized to Cu^{+}, and the same displacement mechanism, aided by the spherical morphology, enables fast and clean Bi dissolution. Together, these effects result in excellent switching speed, reversibility, and cycling stability achieved in our work.

In contrast, a Bi-based RME device with the Bi-only electrolyte exhibits poor switching speed, reversibility, and cycling stability (**Figure R7**). Even after 120 s of deposition, the device still has a solar transmittance (T_{sol}) of over 5% (**Figure R7a**), indicating slow switching speed. After only 10 cycles, non-uniform deposition and incomplete stripping are observed (**Figure R7b**), reflecting poor reversibility arising from the dendritic growth morphology of pure Bi deposits (**Figure R7c**). This is further supported by a charge imbalance between deposition and stripping in the chronoamperometric curve (**Figure R7d**). As a result, the device retains only 22.5% of its initial contrast after 50 cycles (**Figure R7e**), demonstrating extremely limited cycling stability.

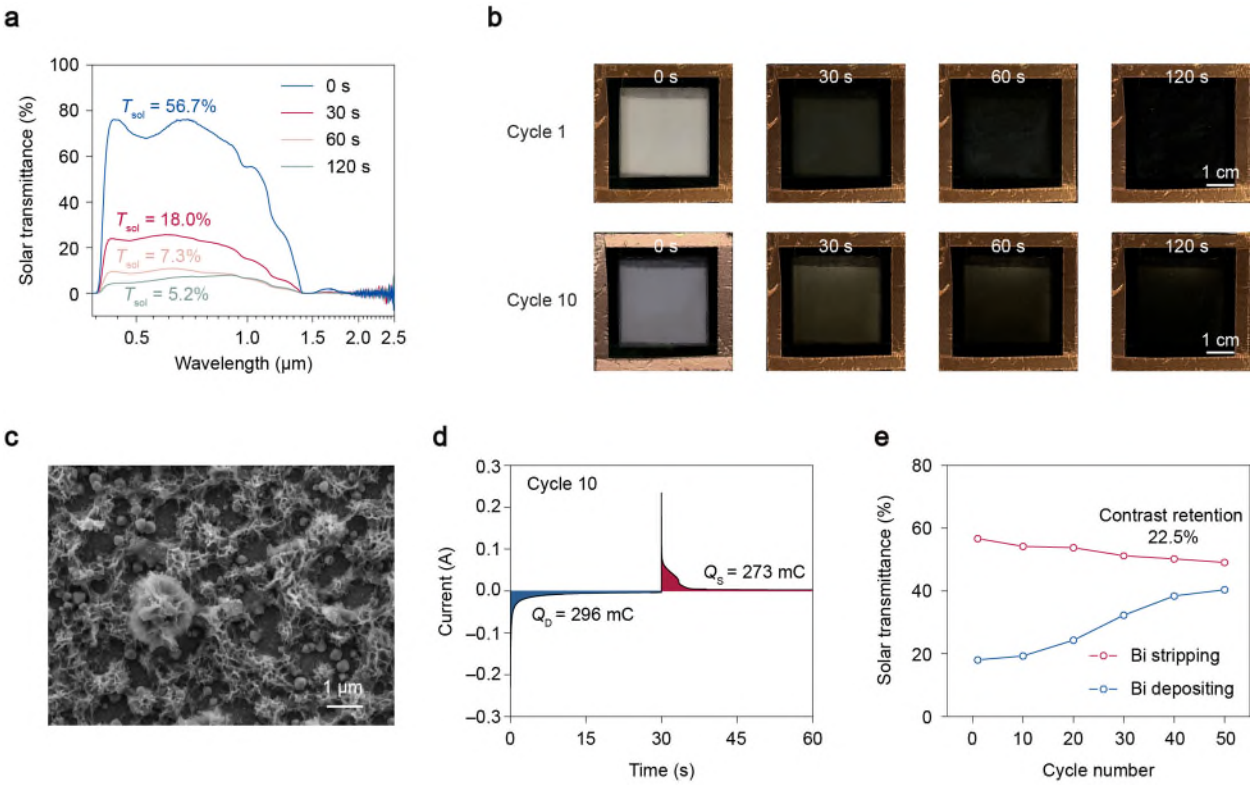

Figure R7. Electrochromic performance of a Bi-based RME device using the Bi-only electrolyte. **a**, Solar transmittance spectra recorded at different depositing times. **b**, Optical photographs of the device at cycle 1 and 10 for various depositing times. **c**, SEM images of the deposited Bi films at cycle 10, revealing a dendritic morphology. **d**, Chronoamperometric curve exhibiting the charge imbalance between deposition and stripping. **e**, Cycling performance of the deices across the solar spectrum.

[Changes in revised manuscript]:

We have made three main changes in the revised manuscript and SI.

1. Page 6 of the revised manuscript.

We added a discussion to highlight the excellent electrochemical reversibility and stable cycling performance of the Cu–Bi film throughout its formation and removal:

"*As an illustrative example, we applied Cu–bismuth (Cu–Bi) as the black RME material (Fig. 1b, right) due to its excellent electrochemical reversibility and stable cycling performance (Supplementary Note 2), which can be expanded to other metal films with strong plasmonic absorption, such as Cu–zinc (Cu–Zn)*[35]*, Cu*[45] *or silver (Ag)*[46] *under controlled conditions.*"

2. Page 25 of the revised SI.

We linked the deposition and stripping processes of the Cu–Bi film to the current–time curve:

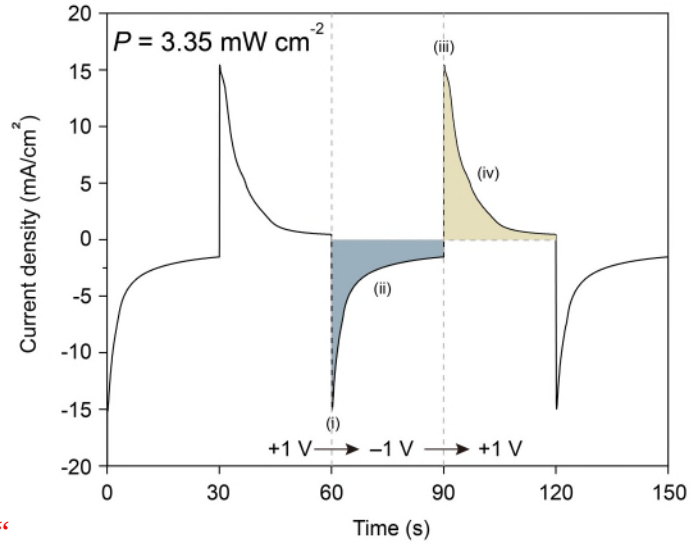

“

Supplementary Fig. 24: Chronoamperometric curve of the STDEC window. The current–time curve shows the distinct stages of the Cu–Bi film deposition and stripping: (i) instantaneous nucleation of Cu–Bi clusters; (ii) concurrent nucleation and growth; (iii, iv) stripping and dissolution of the Cu–Bi film. These symmetric peaks (charge ~100.5 mC/cm^2) indicate excellent electrochemical reversibility and stable cycling performance, with an average power consumption of 3.35 mW cm^{-2}.”

3. Page 57–60 of the revised SI.

We added a supplementary note to clarify the formation and removal of the Cu–Bi film:

“***Supplementary Note 2. Formation and removal mechanism of the Cu–Bi film.***

This section elucidates the formation and removal mechanism of the Cu–Bi film under applied bias and cycling conditions. Supplementary Figure 46 shows the cyclic voltammetry (CV) curve for the deposition and stripping of the Cu–Bi film, obtained within a voltage range of –1.0 V to +1.0 V at 50 mV/s. During the initial negative-going sweep, the cathodic current starts to rise at 0.52 V, attributed to the reduction of Cu^{2+} to Cu^{+} without any metal deposition. A further increase in cathodic current at –0.2 V, corresponds to the reduction of Bi^{3+} to Bi and Cu^{+} to Cu. At this phase, Cu^{+} can participate in galvanic displacement reactions with dendritic Bi atoms and fill in void spaces with three times the number of Cu atoms, resulting in a more condensed spherical morphology that suppresses dendritic growth (Supplementary Fig. 47).

During the subsequent positive-going sweep, the negative current indicates the continued reduction of metal ions to Cu–Bi films deposited on the working electrode. Anodic current begins to increase at –0.1 V, due to the dissolution of the Cu and Bi back to Cu^{+} and Bi^{3+}, respectively. At this stage, Cu^{+} can also speed up the dissolution of Bi via galvanic displacement reactions, leaving no residual dead Bi (Supplementary Fig. 47). Cu^{+} is then further oxidized to Cu^{2+} at voltages more positive than 0.65 V.

These deposition and stripping processes can be linked to the current–time curve (Supplementary Fig. 24). When a negative voltage (–1.0 V) is applied, the current–time curve exhibits a transient current peak (Supplementary Fig. 24, i), indicating the instantaneous nucleation of Cu–Bi clusters on the electrode surface. After this peak, the current slowly decays and reaches a diffusion-controlled plateau phase (Supplementary Fig. 24, ii), reflecting the concurrent nucleation and growth of the Cu–Bi film. When the bias is reversed to +1.0 V, a reverse anodic current peak appears (Supplementary Fig. 24, iii) and then gradually diminishes (Supplementary Fig. 24, iv), which corresponds to the stripping and dissolution of the Cu–Bi film. These symmetric peaks, with a charge of about 100.5 mC/cm^2, indicate excellent electrochemical reversibility and stable cycling performance of the Cu–Bi film.

Cu^{2+} critically governs the deposition and stripping of Cu–Bi films, determining switching speed, reversibility, and cycling stability. Upon deposition, Cu^{2+} is reduced to Cu^{+}, which drives galvanic displacement of Bi and promotes the nucleation and growth of spherical particles. Upon stripping, Cu is oxidized to Cu^{+}, and the same displacement mechanism, aided by the spherical morphology, enables fast and clean Bi dissolution. Together, these effects result in excellent switching speed, reversibility, and cycling stability achieved in our work.

In contrast, a Bi-based RME device with the Bi-only electrolyte exhibits poor switching speed, reversibility, and cycling stability (Supplementary Fig. 48). Even after 120 s of deposition, the device still has a solar transmittance (T_{sol}) of over 5% (Supplementary Fig. 48a), indicating slow switching speed. After only 10 cycles, non-uniform deposition and incomplete stripping are observed (Supplementary Fig. 48b), reflecting poor reversibility arising from the dendritic growth morphology of pure Bi deposits (Supplementary Fig. 48c). This is further supported by a charge imbalance between deposition and stripping in the chronoamperometric curve (Supplementary Fig. 48d). As a result, the device retains only 22.5% of its initial contrast after 50 cycles (Supplementary Fig. 48e), demonstrating extremely limited cycling stability.

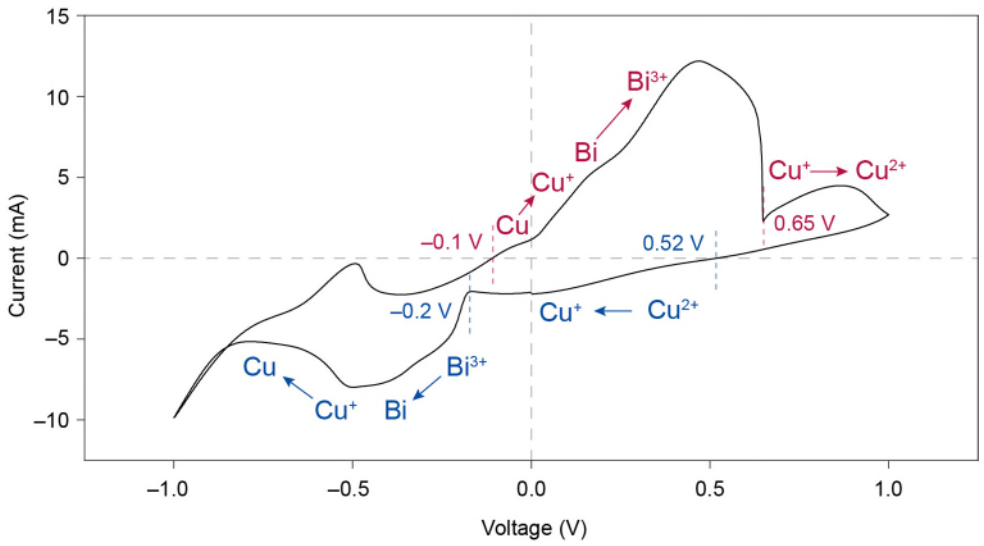

Supplementary Fig. 46: Cyclic voltammogram of the Cu–Bi film measured between –1.0 V and +1.0 V at 50 mV/s.

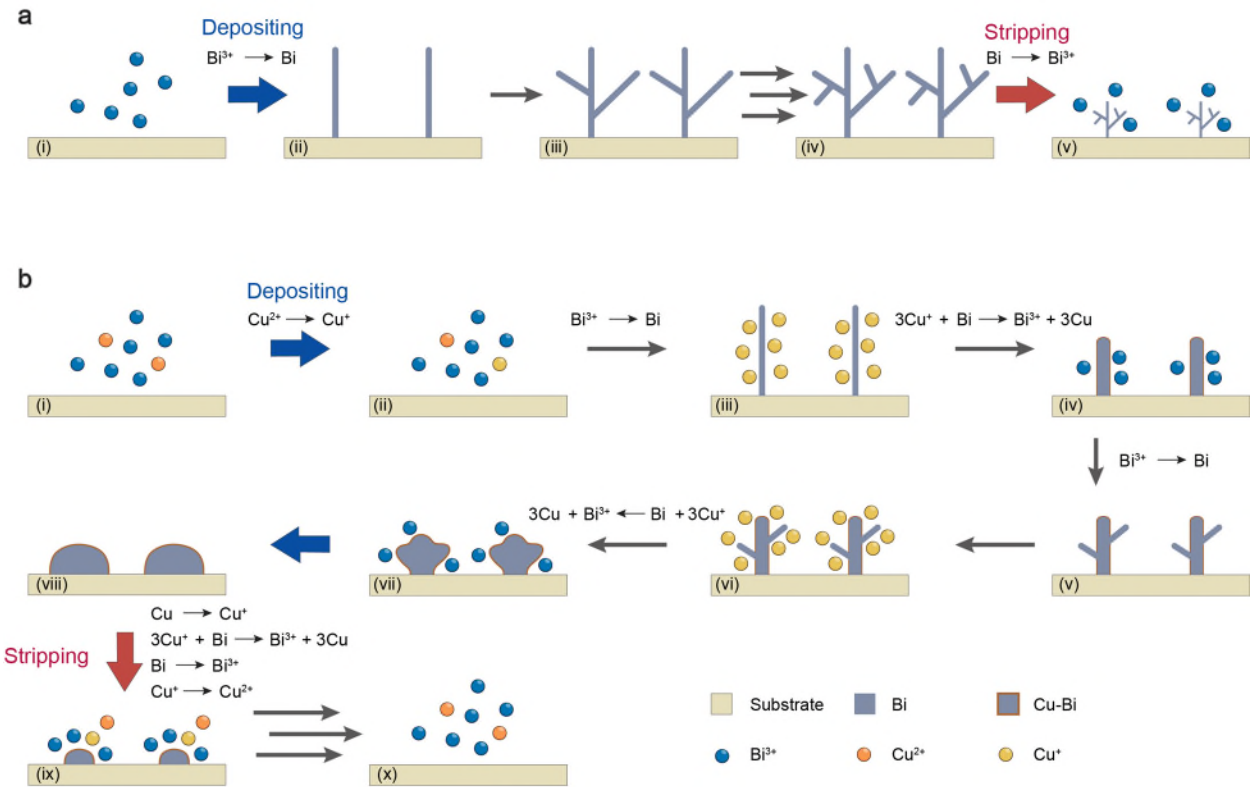

Supplementary Fig. 47: Reaction schematic for the deposition and stripping of Bi films in the (**a**) absence and (**b**) presence of Cu^{2+}.

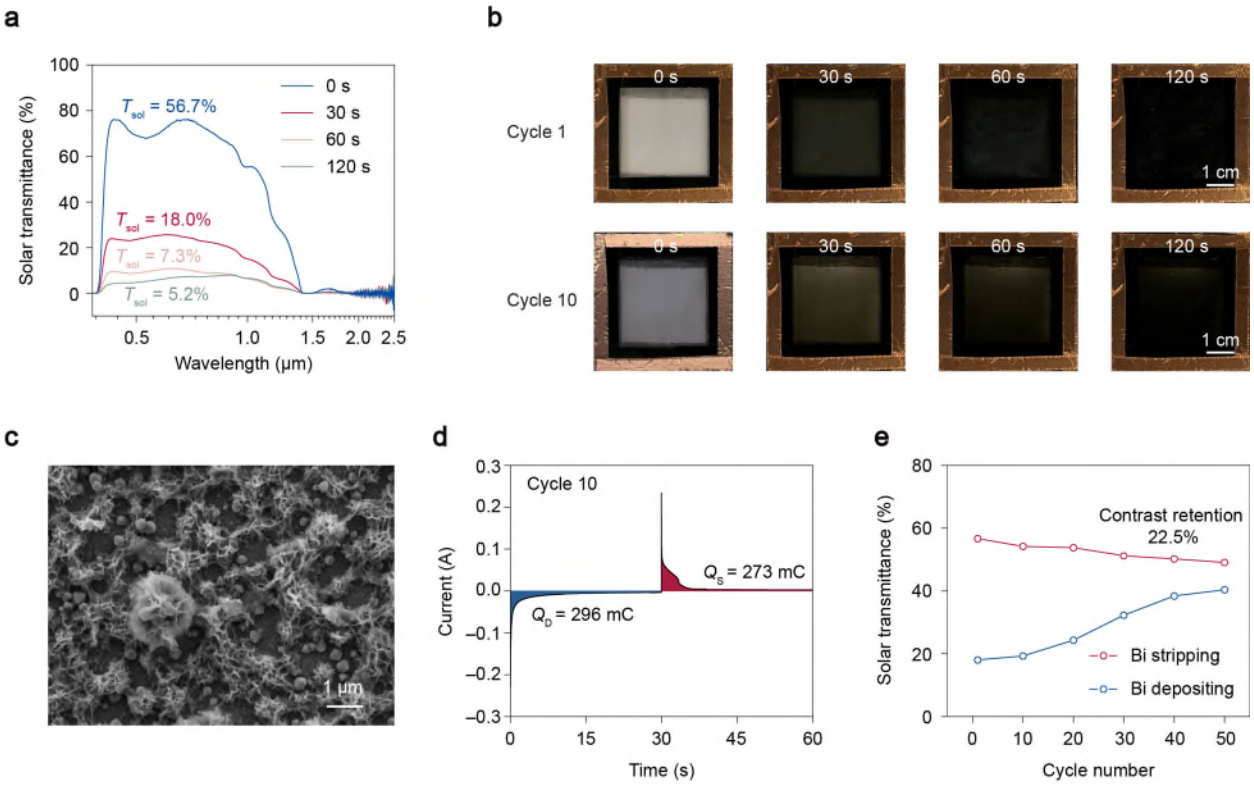

Supplementary Fig. 48: Electrochromic performance of a Bi-based RME device using the Bi-only electrolyte. **a**, Solar transmittance spectra recorded at different depositing times. **b**, Optical photographs of the device at cycle 1 and 10 for various depositing times. **c,** SEM images of the deposited Bi films at cycle 10, revealing a dendritic morphology. **d**, Chronoamperometric curve exhibiting the charge imbalance between deposition and stripping. **e**, Cycling performance of the deices across the solar spectrum."

[Comment 4]: While Fig. 2g demonstrates that the deposited (colored) state remains stable for 36 hours under open-circuit conditions, the stability/retention time of the transparent state is not reported. Please provide quantitative data for how long the transparent state is maintained under open-circuit conditions, and clarify the practical/experimental procedure followed for the stripping process.

[Response]: We thank the reviewer for this constructive suggestion. We have quantified the retention time of the transparent state under open-circuit conditions. Specifically, after applying +1 V for 60 s to fully strip the Cu–Bi film and achieve the transparent state, the bias was removed and the device was maintained under open-circuit conditions. The solar transmittance (T_{sol}) was measured at different intervals over a 36-hour timeframe. The transparent state remained stable

with virtually no variation in transmittance observed during the entire **36 hours** (**Figures R8** and **R9**).

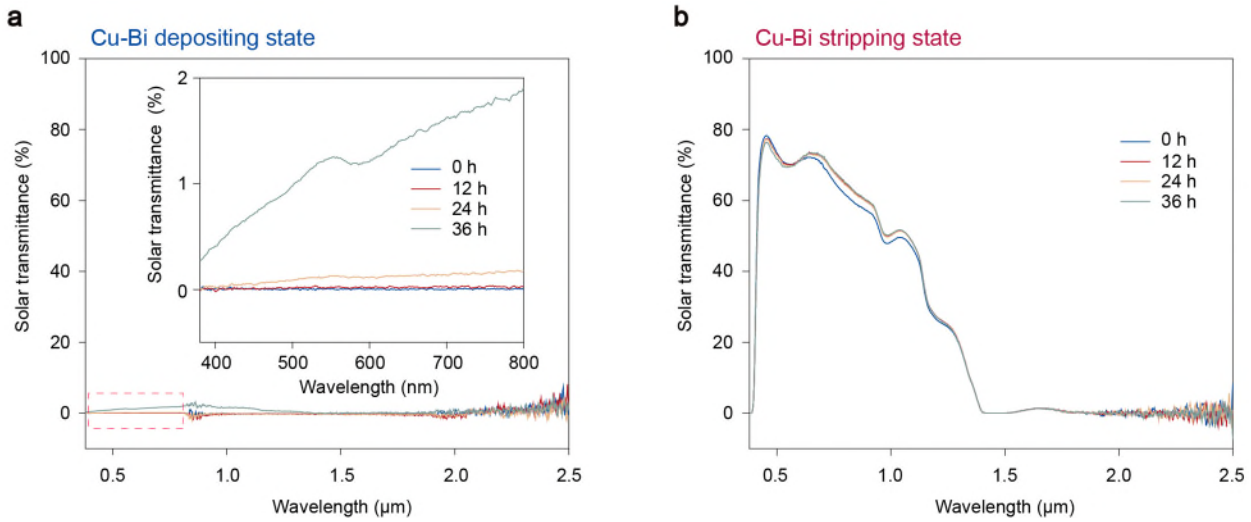

Figure R8. Bistability of the STDEC window. Optical monitoring of the STDEC window in the (**a**) colored (depositing) and (**b**) transparent (stripping) states were conducted under open-circuit conditions for 36 hours. Excellent bistability is observed, with an optical loss of less than 2% in the colored state and no measurable loss in the transparent state.

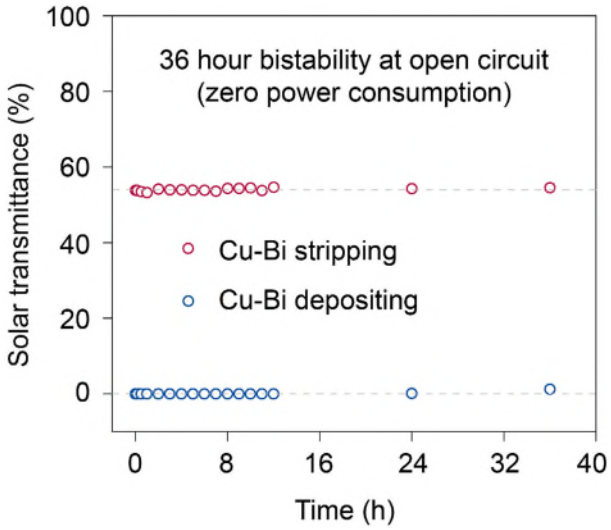

Figure R9. Bistability of the STDEC window across the solar spectrum. Optical transmittance monitoring of the STDEC window at the black and clear states and left at open-circuit for 36 hours with zero power consumption.

[Changes in revised manuscript]:

We have made one main change in the revised manuscript and SI.

1. Page 11 of the revised manuscript.

We revised the sentence to highlight the stability time of the transparent state:

"In the open-circuit state, the STDEC window can keep its black state for a staggering 36 hours with less than 2% optical loss and its clear state for the same duration without any optical loss (Fig. 2g and Supplementary Fig. 23), indicating the extra electrical power is negligible to maintain its optical state.

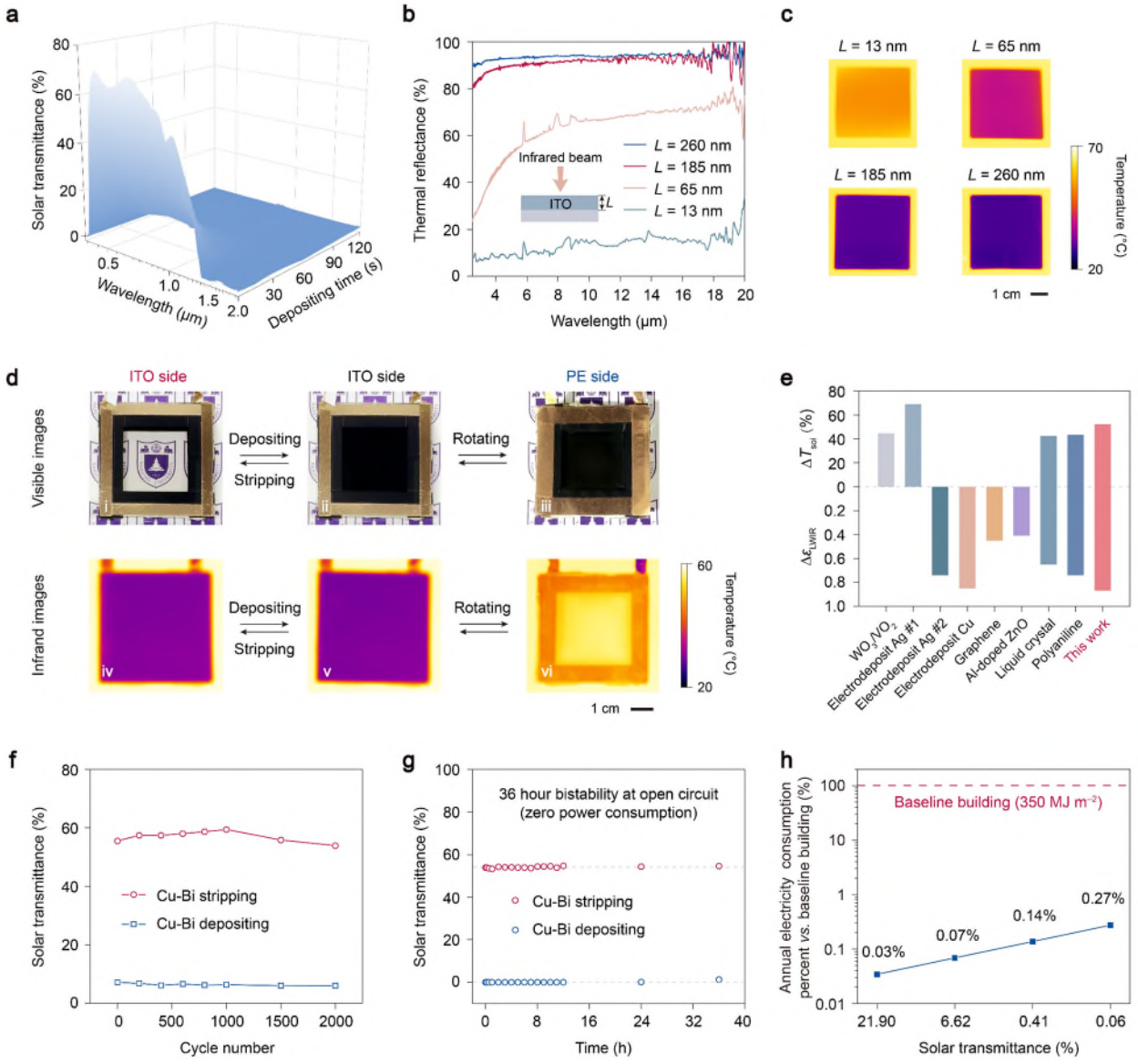

Fig. 2 | Optical and thermal properties of the STDEC window. a, Solar transmittance spectra recorded at various depositing times. **b**, Effect of the thickness of the ITO layer on its thermal reflectance. **c**, Infrared images of the ITO layer at different thicknesses taken on the same hot plate. **d**, Optical photographs and thermal images of the STDEC window showing both independent and synergistic regulation on solar and thermal ranges. **e**, Comparison of various EC strategies for modulating T_{sol} and ε_{LWIR}[25,27–30,42,47,48]. **f**, Cycling performance of the STDEC window across the solar spectrum. **g**, Bistability of the STDEC window across the solar spectrum. Optical transmittance monitoring of the STDEC window at the black and clear states and left at open-circuit for 36 hours with zero power consumption. **h**, The percentage of annual electricity consumption for the STDEC window switching between various optical states compared to the yearly electricity usage of a baseline building.

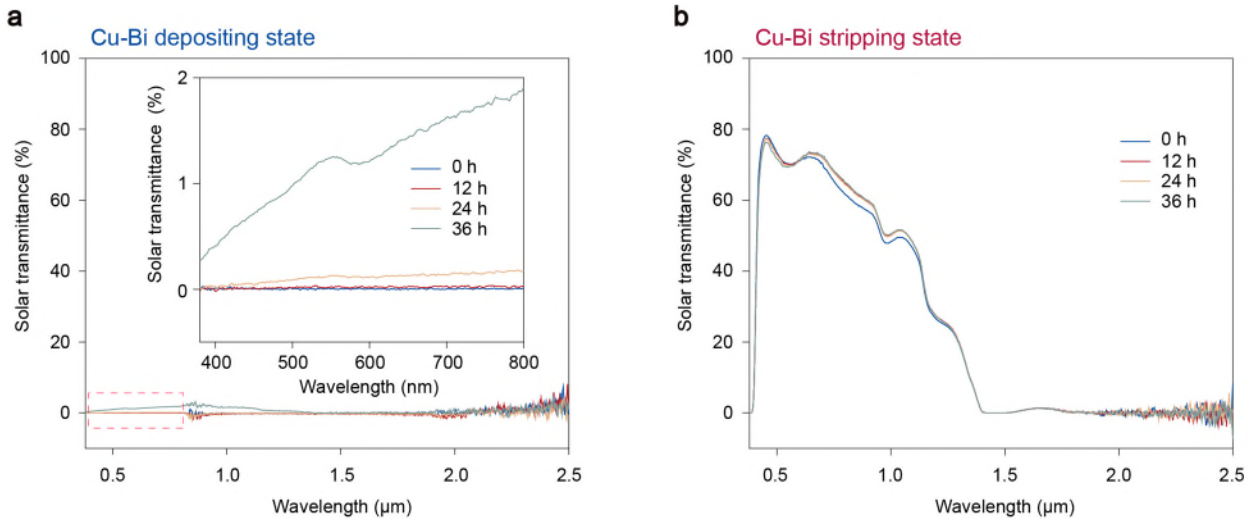

Supplementary Fig. 23: Bistability of the STDEC window. Optical monitoring of the STDEC window in the (**a**) colored (depositing) and (**b**) transparent (stripping) states were conducted under open-circuit conditions for 36 hours. Excellent bistability is observed, with an optical loss of less than 2% in the colored state and no measurable loss in the transparent state."

[Comment 5]: Is it possible to achieve additional coloration states or hues by modifying the electrolyte composition or pH, or through structural changes to the device? Can the electrolyte thickness be controlled systematically, and if so, how does this influence switching performance, including speed, efficiency, or color contrast?

[Response]: We thank the reviewer for this insightful question. We have explored the possibility of achieving additional coloration states or hues by modifying the device structure and electrolyte conditions. **First**, by employing a bare ITO electrode (without Pt nanoparticle modification) and a step potential protocol (applying –1.6 V for 10 ms, then –1.0 V for 200 s), we achieved additional coloration states different from black (**Figure R10**). This demonstrates that altering the electrode structure together with tailored voltage control can generate a broader range of colors. **Second**, we changed the pH of the electrolyte. However, across all the pH levels tested, the device continued to switch solely between transparent and black states (**Figure R11**), without showing any other distinct hues.

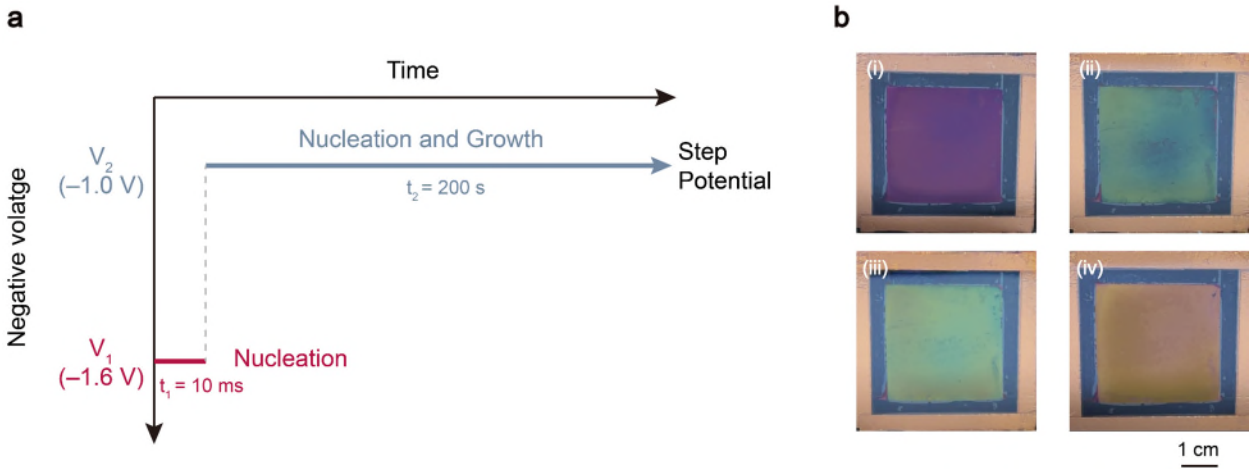

Figure R10. a, Schematic of a deposition strategy based on the step potential protocol. **b**, Optical photographs of additional hues generated on the bare ITO electrode via the step potential protocol.

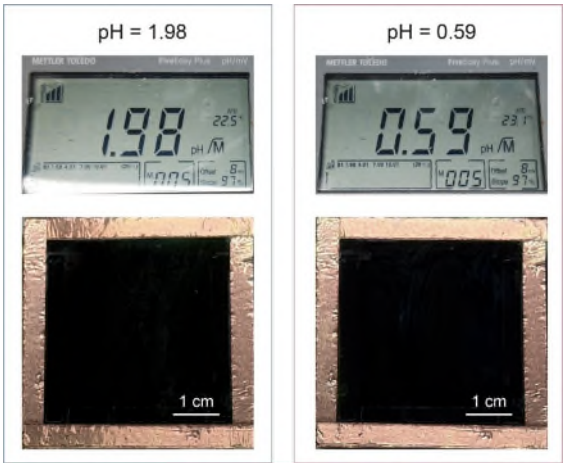

Figure R11. Optical photographs of the pH values of the altered electrolyte and the corresponding devices in their black states.

The electrolyte thickness can be systematically controlled by adjusting the spacer layer in the device configuration. **Figure R12** presents optical images of devices featuring varied electrolyte thicknesses (e.g., **1 mm**, **2 mm**, and **4 mm**), alongside their solar transmittance spectra measured at different depositing times. Notably, no significant variation in the spectral performance was observed across the different thicknesses, suggesting that electrolyte thickness has minimal impact on switching speed, efficiency, and color contrast.

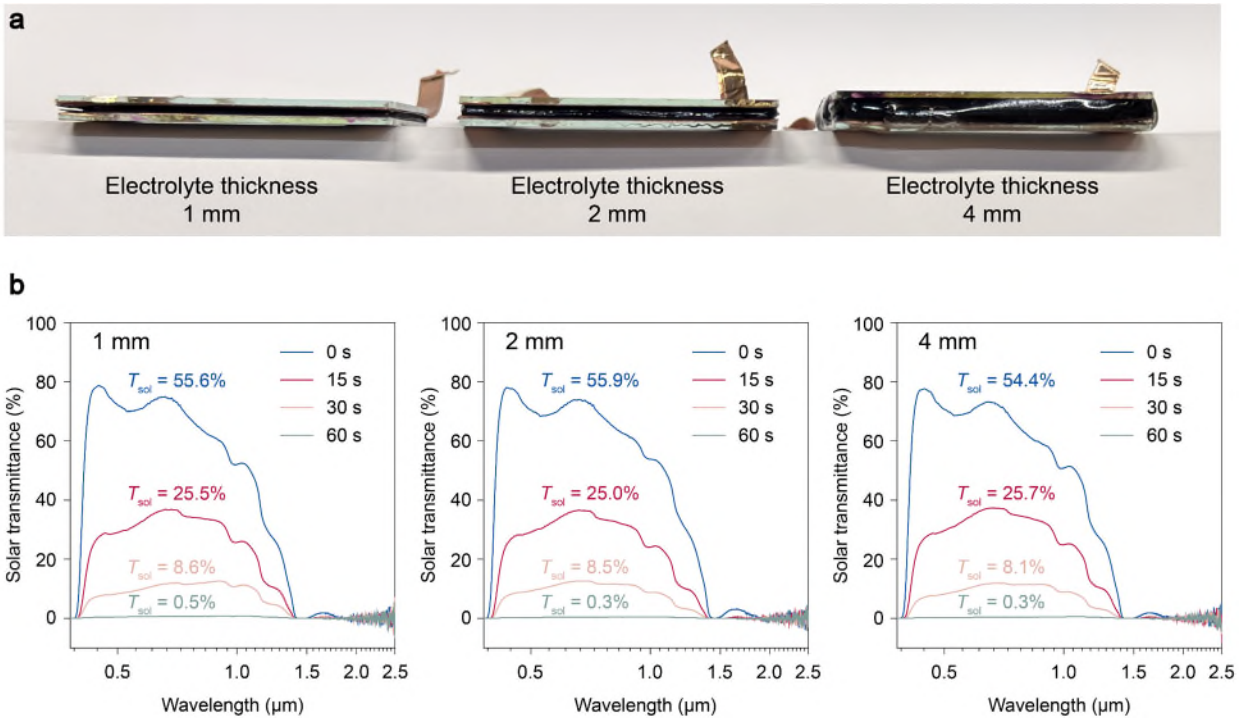

Figure R12. Optical photographs (**a**) and solar transmittance spectra at different depositing times (**b**) of devices with electrolyte thicknesses of 1 mm, 2 mm, and 4 mm.

[Comment 6]: In the vertical thermal cycling test, normal glass and low-E glass show pronounced temperature fluctuations, while STDEC and EC samples do not. Please clarify which physical or material properties of the STDEC/EC windows are responsible for this effect—e.g., thermal insulation, emissivity, or other factors.

[Response]: We thank the reviewer for this important comment. We would like to clarify that the observed difference in temperature fluctuations in the vertical thermal cycling test (**Figure R13a**) arises primarily from the **distinct solar transmittance of the windows**. During daytime, the solar irradiance fluctuates substantially from 12:00 to 14:00 on 18 September 2024 (**Figure R13b**).

Normal glass and low-E glass have high solar transmittance, allowing a large fraction of incident solar radiation to pass through and heat the interior space. As a result, their temperatures closely track changes in solar irradiance, leading to pronounced temperature fluctuations.

In contrast, the STDEC/EC windows exhibit extremely low solar transmittance (T_{sol} <0.1%) in their colored states, blocking nearly all the incoming solar radiation and resulting in significantly minimal temperature variations against external solar irradiance fluctuations.

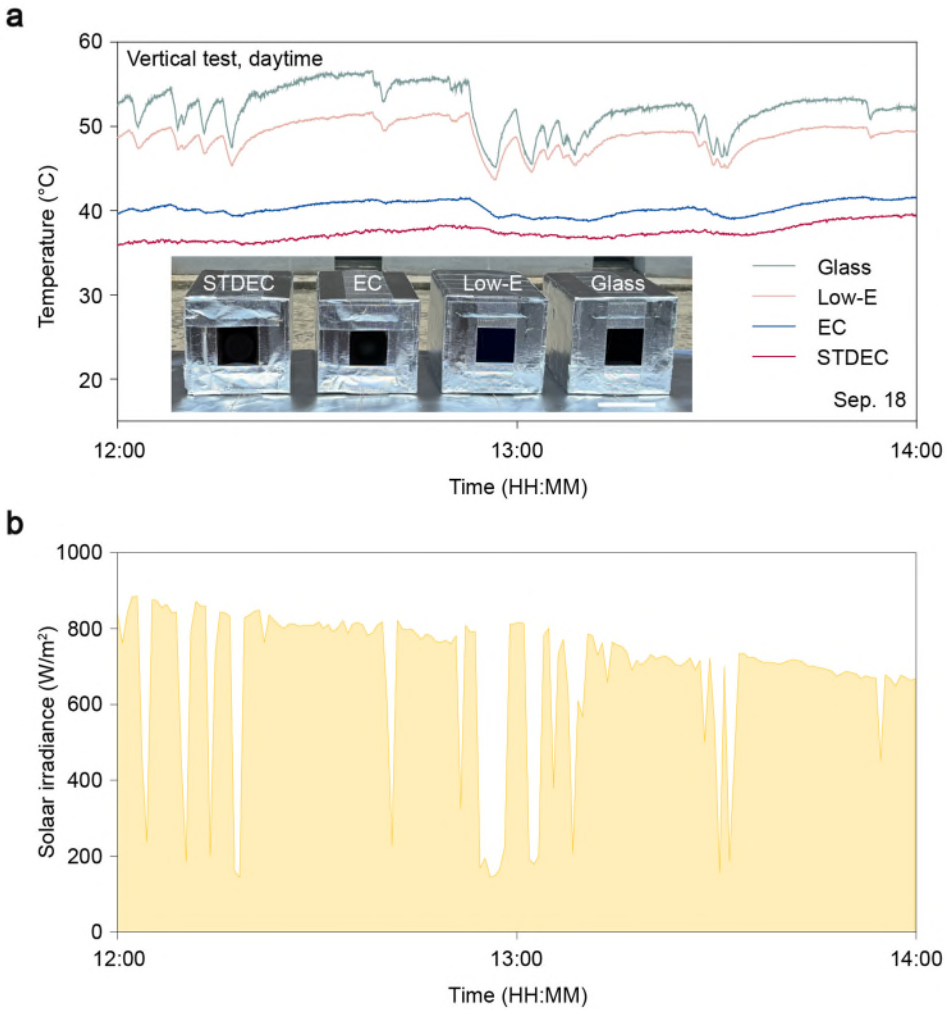

Figure R13. Vertical temperature measurements. **a**, Temperature tracking of different vertically oriented samples measured from 12:00 to 14:00 on 18 September 2024. The inset is an apparatus photograph showing the measurement setup for vertically oriented samples. Scale bars, 10 cm. **b**, Solar irradiance from 12:00 to 14:00 on 18 September 2024.

[Changes in revised manuscript]:

We have made one main change in the revised manuscript and SI.

1. Page 38 of the revised SI.

We added the solar irradiance data from 12:00 to 14:00 on 18 September 2024 in the revised Supplementary Fig. 36:

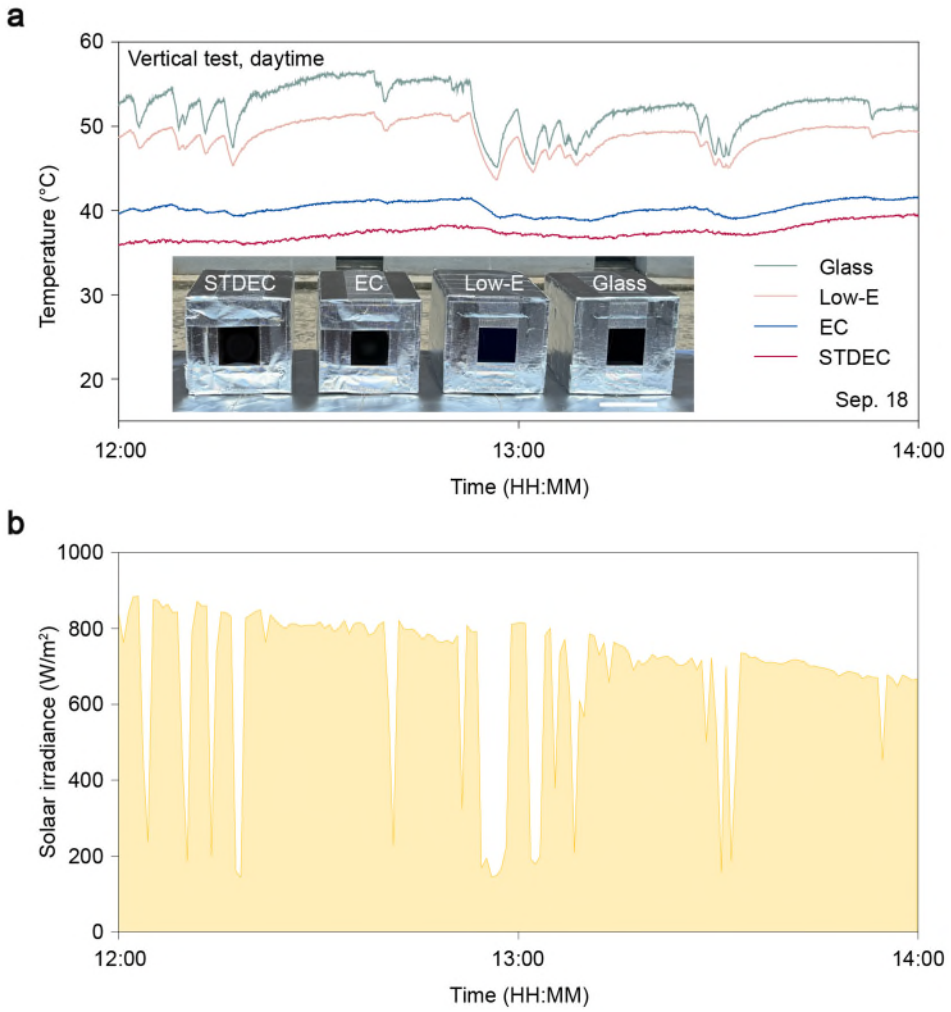

“

Supplementary Fig. 36: Vertical temperature measurements. **a**, Temperature tracking of different vertically oriented samples measured from 12:00 to 14:00 on 18 September 2024. The inset is an apparatus photograph showing the measurement setup for vertically oriented samples. Scale bars, 10 cm. **b**, Solar irradiance from 12:00 to 14:00 on 18 September 2024.”

Response to Reviewer 2

[General Comment]: The manuscript reports a solar and thermal dual-band electrochromic smart window capable of modulating both solar transmission and long-wave infrared emissivity, thereby enabling all-season control of building energy. The approach integrates a reversible metal electrodeposition electrochromic system with a mechanical rotation mechanism to independently control solar transmittance and thermal emissivity. The concept is novel and significant in the field of smart windows. The approach is both conceptually innovative and practically impactful. While I would be happy to recommend it for publication, there are a few concerns that need to be addressed to further improve the manuscript.

[Response]: We sincerely thank Reviewer 2 for the positive recognition of our work and for **recommending publication**. Based on the valuable comments, we have made revisions that further enhance the quality of the manuscript.

[Comment 1]: While the RME cycling stability is well documented for 2000 cycles, the long-term performance under environmental stress remains insufficiently addressed. How does the electrolyte hold up under extended UV exposure, weathering, or temperature/humidity cycling?

[Response]: We thank the reviewer for this important concern. To assess the long-term stability of the electrolyte under environmental stress, we have performed additional cycling measurements under extended UV exposure (**Figure R14**), weathering (**Figure R15**), and temperature/humidity cycling (**Figure R16**) conditions. Under all tested conditions, the device maintained an optical contrast exceeding 90% after 1,000 cycles, demonstrating robust environmental durability.

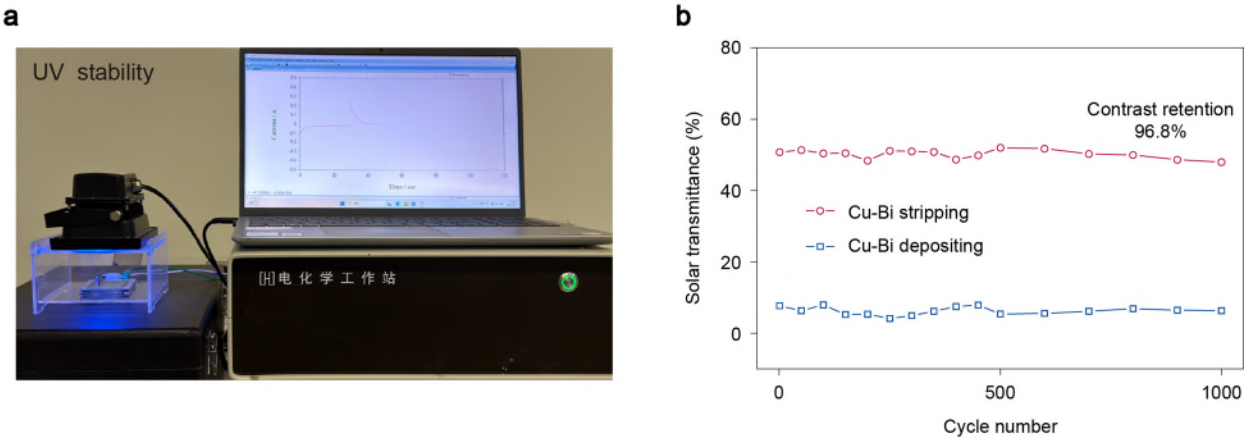

Figure R14. UV stability. **a**, Photograph of the experimental setup for extended UV exposure at 640 W m^{-2}. **b**, Cycling stability over 1,000 cycles, showing 96.8% retention of optical contrast.

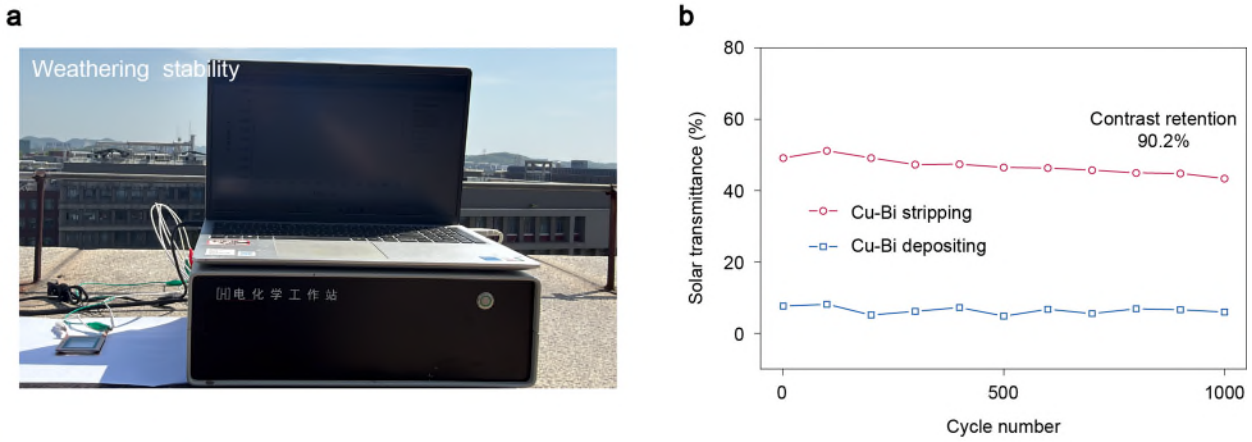

Figure R15. Outdoor weathering stability. **a**, Photograph of the experimental setup for outdoor weathering test. **b**, Cycling stability over 1,000 cycles, showing 90.2% retention of optical contrast.

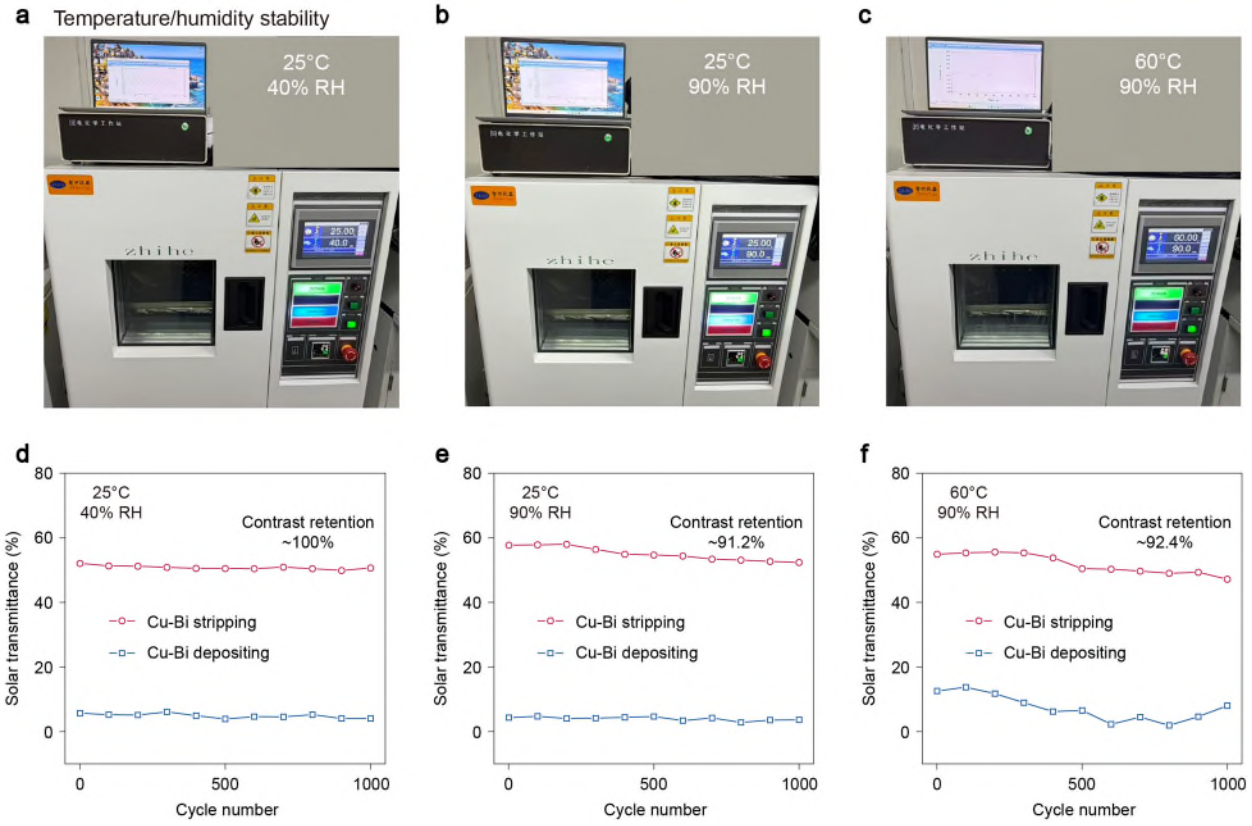

Figure R16. Temperature/humidity stability. **a–c**, Photographs of the experimental setup for temperature/humidity cycling tests in a constant temperature and humidity chamber under 3 conditions: 25℃/40% RH (**a**), 25℃/90% RH (**b**), and 60℃/90% RH (**c**). **d–f**, Corresponding cycling stability over 1,000 cycles, with optical contrast retention of ~100% (**d**), 91.2% (**e**), and 92.4% (**f**).

[Changes in revised manuscript]:

We have made three main changes in the revised manuscript and SI.

1. Page 11 of the revised manuscript.

We added a sentence to highlight the cycling stability under environmental stress:

"*Even under environmental stresses such as extended UV exposure (Supplementary Fig. 18), weathering (Supplementary Fig. 20), and temperature/humidity fluctuations (Supplementary Fig. 21), the STDEC window retains over 90% of its optical contrast after 1,000 cycles, demonstrating robust environmental durability.*

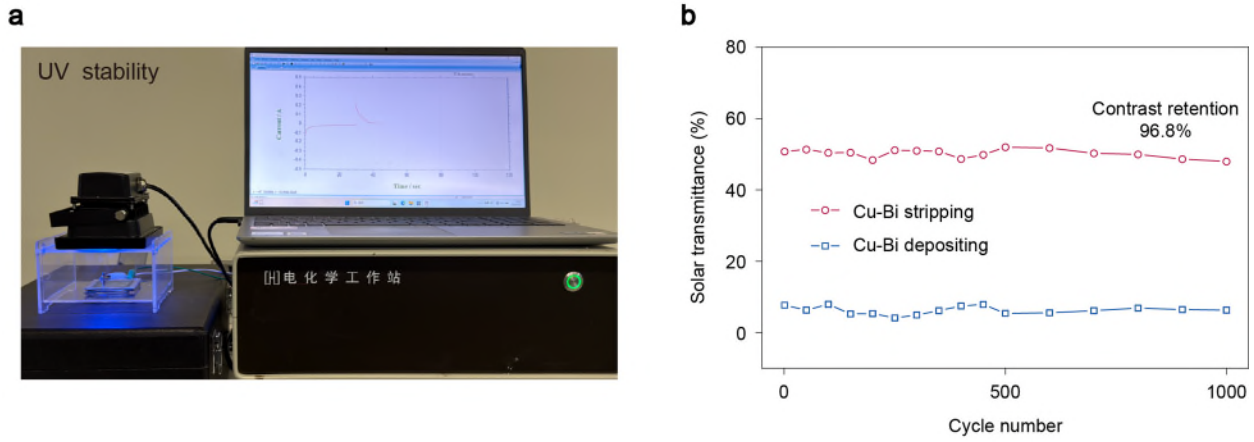

Supplementary Fig. 19: UV stability. **a**, Photograph of the experimental setup for extended UV exposure at 640 W m^{-2}. **b**, Cycling stability over 1,000 cycles, showing 96.8% retention of optical contrast.

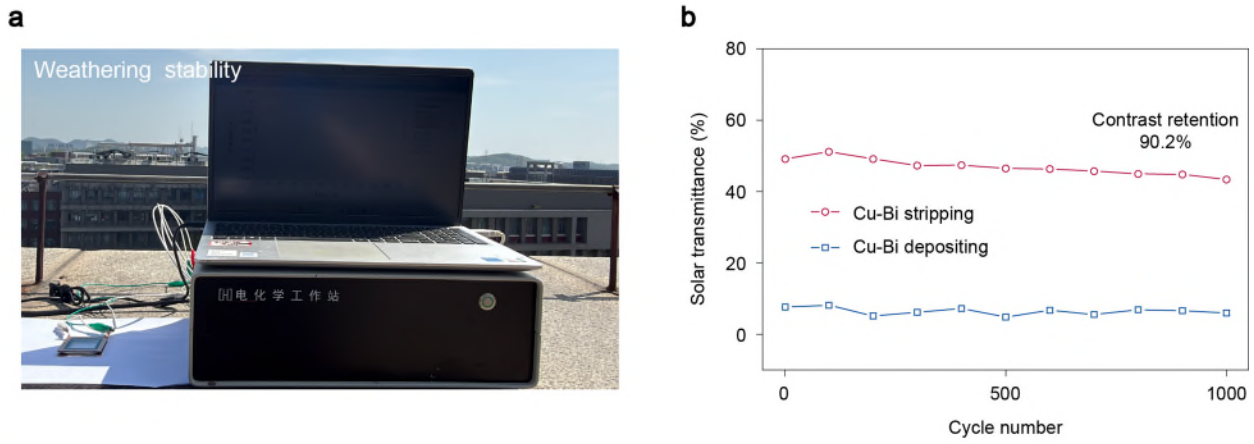

Supplementary Fig. 20: Outdoor weathering stability. **a**, Photograph of the experimental setup for outdoor weathering test. **b**, Cycling stability over 1,000 cycles, showing 90.2% retention of optical contrast.

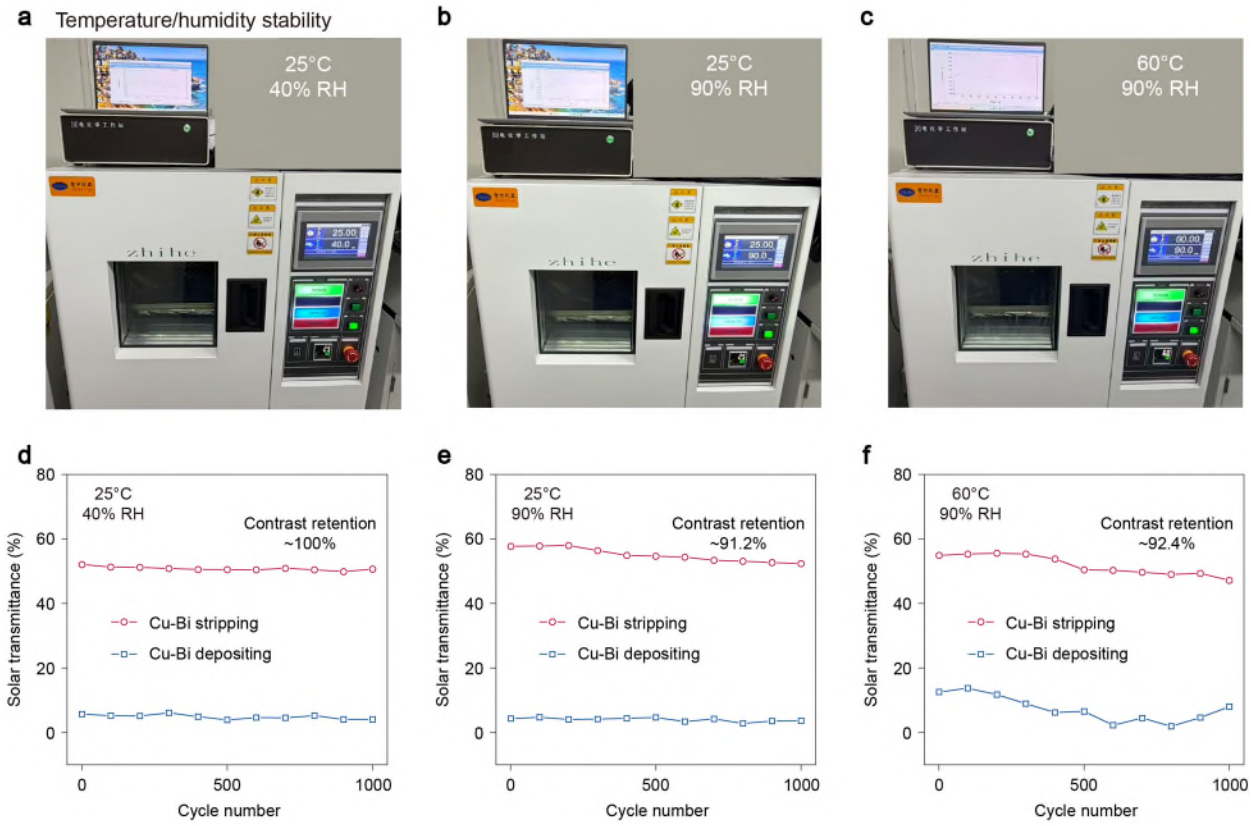

Supplementary Fig. 21: Temperature/humidity stability. **a–c**, Photographs of the experimental setup for temperature/humidity cycling tests in a constant temperature and humidity chamber under 3 conditions: 25℃/40% RH (**a**), 25℃/90% RH (**b**), and 60℃/90% RH (**c**). **d–f**, Corresponding cycling stability over 1,000 cycles, with optical contrast retention of ~100% (**d**), 91.2% (**e**), and 92.4% (**f**)."

2. Page 19 of the revised manuscript.

In the **Discussion** section, we have added a forward-looking perspective. Future work will explore the long-term performance of the electrolytes under extreme environmental conditions to facilitate global implementation of the windows:

"*Despite its advantages, the STDEC window requires further improvements in operational stability, environmental durability and lifetime. Exploring alternative electrolytes represents a promising engineering route to extend window durability. In particular, developing electrolytes capable of long-term operation under high UV exposure, high humidity, and extreme high/low temperatures will be crucial for global climate adaptability.*"

3. Page 21 of the revised manuscript.

The "**Material characterization**" section has been updated with a description of cycling stability measurements under extreme environmental conditions:

"*The cycling stability of the device under extreme environmental conditions was evaluated using a 365 nm UV lamp (6 W), and a constant temperature and humidity chamber (THP-150K, Zhihe).*"

[Comment 2]: The soft PE layer on the front side might be fragile to wind/rain/snow/etc. In this work, an outdoor experiment was conducted at very low wind speeds, with an average of 2 m/s. How to protect this device from heavy rain/snow, or strong winds/dust?

[Response]: We thank the reviewer for this insightful comment. We agree that the original PE material used in this work has limited mechanical strength (**Figure R17a**) and may be fragile to outdoor damage from heavy rain/snow, and strong winds/dust. To address this, we **first** replaced it with high-density polyethylene (HDPE), which offers greatly enhanced mechanical robustness (**Figure R17a**) while maintaining comparable spectral modulation performance (**Figure R17b**). **Second**, for more demanding applications, we substituted the PE with poly(methyl methacrylate) (PMMA), which possesses higher mechanical robustness. Notably, the high emissivity of PMMA can replaced that of the electrolyte in the original device architecture, thus preserving the radiative cooling functionality of the device. The resulting PMMA-based STDEC window also exhibits the excellent spectral modulation in both the solar and thermal regions (**Figure R18**).

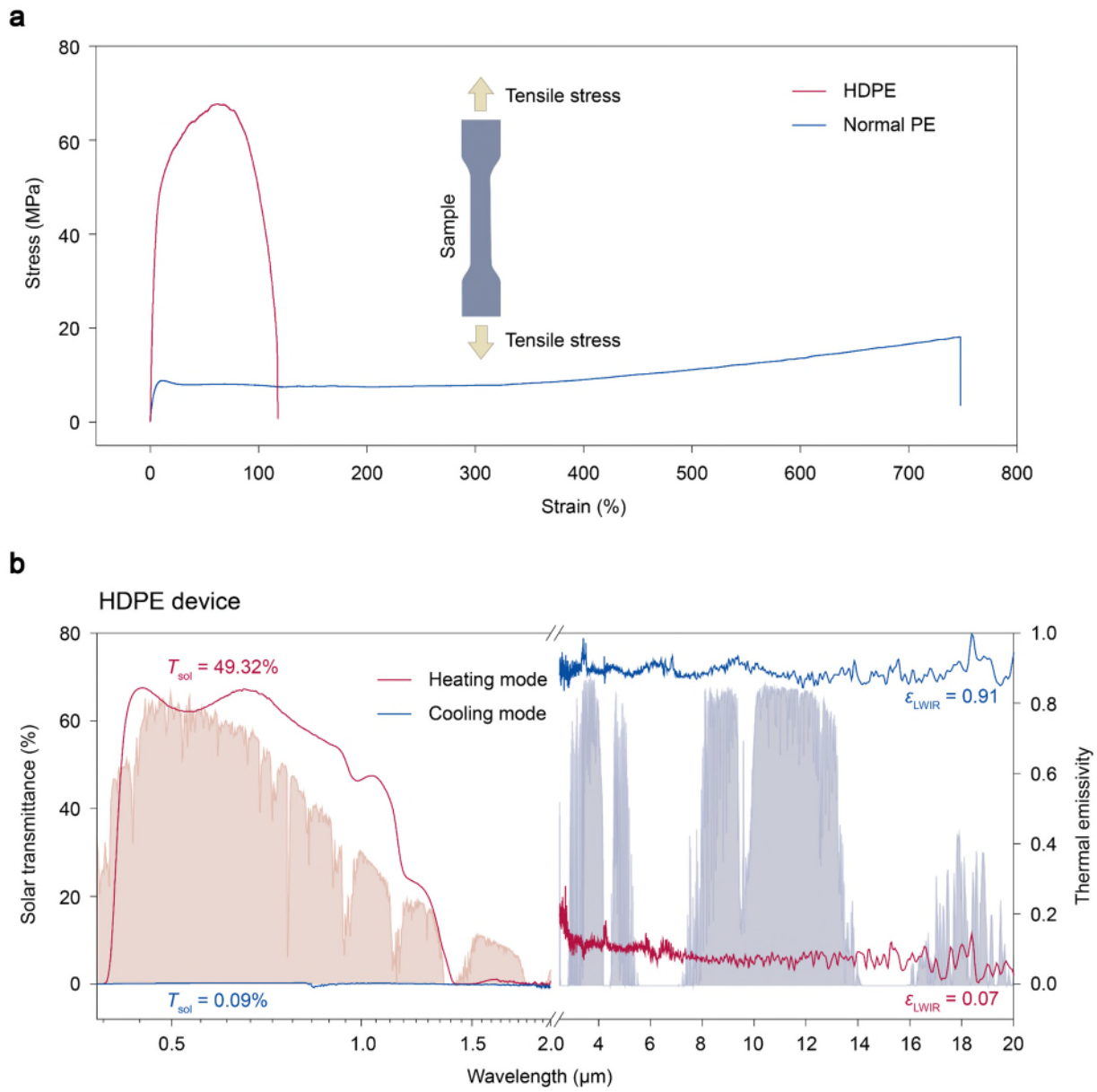

Figure R17. HDPE-based STDEC window. **a**, Mechanical properties of the normal PE and HDPE. **b**, Spectral modulation performance.

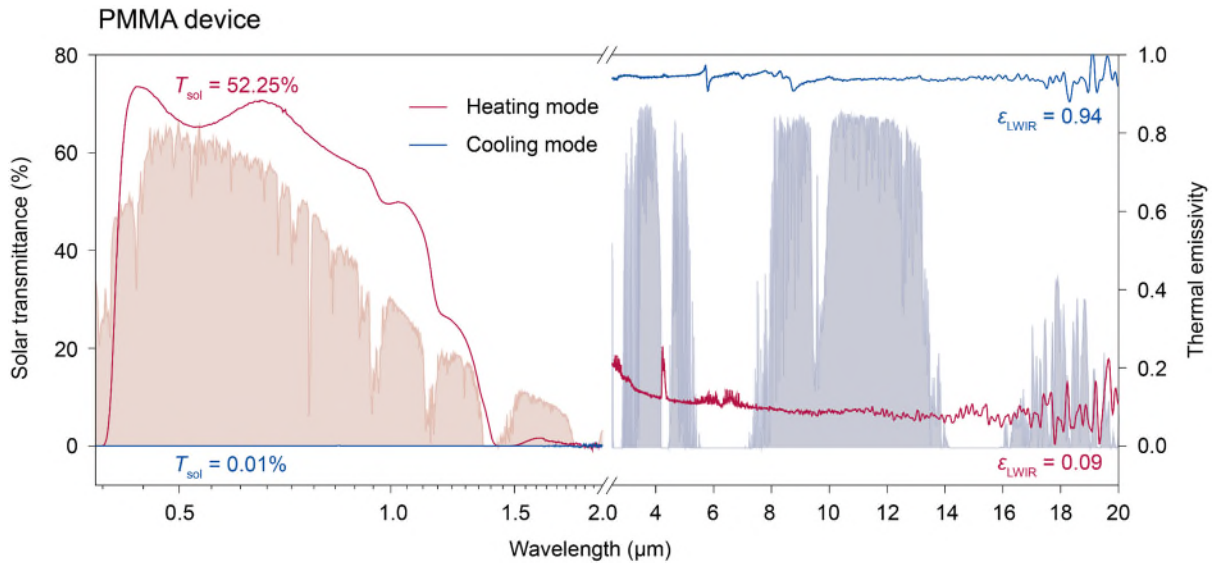

Figure R18. Spectral modulation performance of the PMMA-based STDEC window.

[Comment 3]: The aqueous PVA-based electrolyte might be prone to drying out or freezing in cold climates. Can the authors comment on the layer adhesion and electrode contact in relation to thermal stress between high-heat-gain and deep-cooling cycling states? Also, the electrolyte system is highly corrosive and toxic; does the electrolyte leach out during the same thermal stress?

[Response]: We thank the reviewer for this insightful comment regarding the electrolyte stability under extreme temperatures. We agree that the aqueous PVA-based electrolyte indeed froze when the device was exposed to –45°C for 30 minutes (**Figures R19a** and **b**). However, even after freezing, the device remained capable of electrodeposition upon applying the bias (**Figures R19c–f**), showing that the reversible redox process was not severely impaired.

We then subjected the device to alternating high-heat-gain (**Figure R20**) and deep-cooling (**Figure R19**) cycling states. Despite these thermal stresses, the device consistently exhibited normal deposition currents (**Figures R19d** and **R20c**) and spectral modulation (**Figures R19e** and **R20d**), indicating that the electrode–electrolyte contact and the adhesion of the deposited Cu–Bi film to the ITO layer remained stable (**Figures R19f** and **R20e**). No delamination or contact failure was observed.

Furthermore, we recognize the reviewer's concern regarding potential electrolyte leakage under different thermal stresses, given the corrosive and toxic nature of the electrolyte system. Notably, **no leakage was observed** during any of the thermal cycling tests (**Figures R19b,c** and **R20a,b**), demonstrating that the device preserved its sealing integrity throughout the tests.

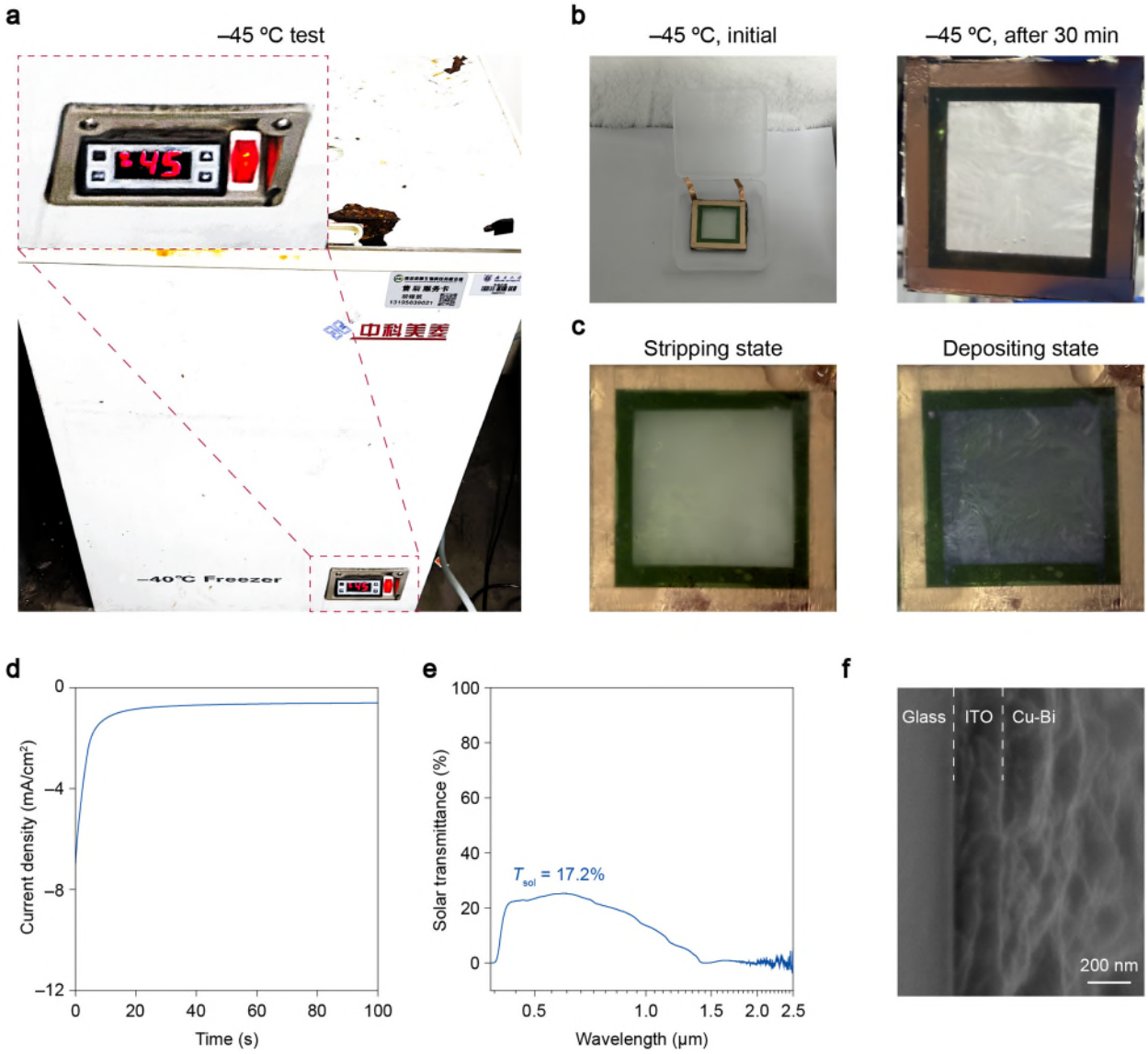

Figure R19. Electrolyte stability at –45°C. **a**, Photograph of the experimental setup for extreme low-temperature test. **b**, Photographs of the device at its initial state and after 30 minutes exposure to –45°C. **c**, Photographs of the device in the stripping and depositing states. **d**, Deposition current of the device at –45°C. **e**, Solar transmittance spectrum of the device in the depositing state. **f**, SEM image of the deposited Cu–Bi film, showing good adhesion to the ITO layer.

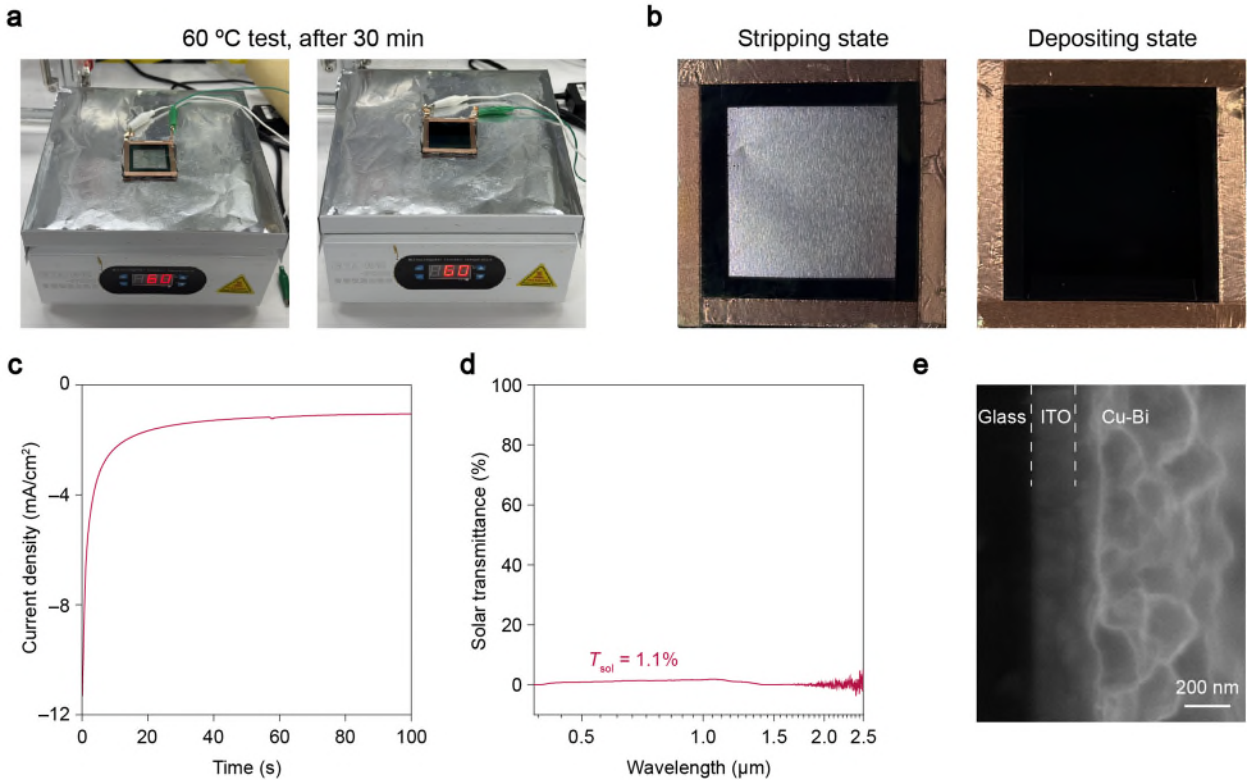

Figure R20. Electrolyte stability at 60°C. **a**, Photograph of the experimental setup for extreme high-temperature test. **b**, Photographs of the device in the stripping and depositing states after 30 minutes exposure to 60°C. **c**, Deposition current of the device at 60°C. **d**, Solar transmittance spectrum of the device in the depositing state. **e**, SEM image of the deposited Cu–Bi film, showing good adhesion to the ITO layer.

[Changes in revised manuscript]:

We have made one main change in the revised manuscript and SI.

1. Page 19 of the revised manuscript.

In the **Discussion** section, we have added a forward-looking perspective. Future work will explore the long-term performance of the electrolytes under extreme environmental conditions to facilitate global implementation of the windows:

"*Despite its advantages, the STDEC window requires further improvements in operational stability, environmental durability and lifetime. Exploring alternative electrolytes represents a promising engineering route to extend window durability. In particular, developing electrolytes capable of long-term operation under high UV exposure, high humidity, and extreme high/low temperatures will be crucial for global climate adaptability.*"

[Comment 4]: Is the STDEC window view distortion-free? Also, the study doesn't mention haze or clarity. The authors should address this.

[Response]: We thank the reviewer for this constructive suggestion. The STDEC window is free from view distortion **(Figure R2**). To quantitatively assess the optical clarity of the window, we calculated the Haze in both the stripping and depositing states using the following formula:

$$\text{Haze (\%)} = \left[\left(\tau_4 / \tau_2 \right) - \tau_3 \left(\tau_2 / \tau_1 \right) \right] \times 100$$

where τ_1 is the total transmittance without the sample (100%); τ_2 is the total transmittance with the sample; τ_3 is the diffuse transmittance without the sample; and τ_4 is the diffuse transmittance with the sample. **Figure R21** presents the total and diffuse transmittance spectra of the STDEC window in the stripping and depositing states, along with the diffuse transmittance spectrum measured without the window sample. All spectra were obtained using an integrating sphere. There is nearly no diffuse transmittance across the solar spectrum, which explains the low measured haze values (Haze = 0.43% at T_{sol} = 55.90%; Haze = 0.82% at T_{sol} = 8.53%; **Table R1**) and demonstrates the excellent optical clarity of the STDEC windows.

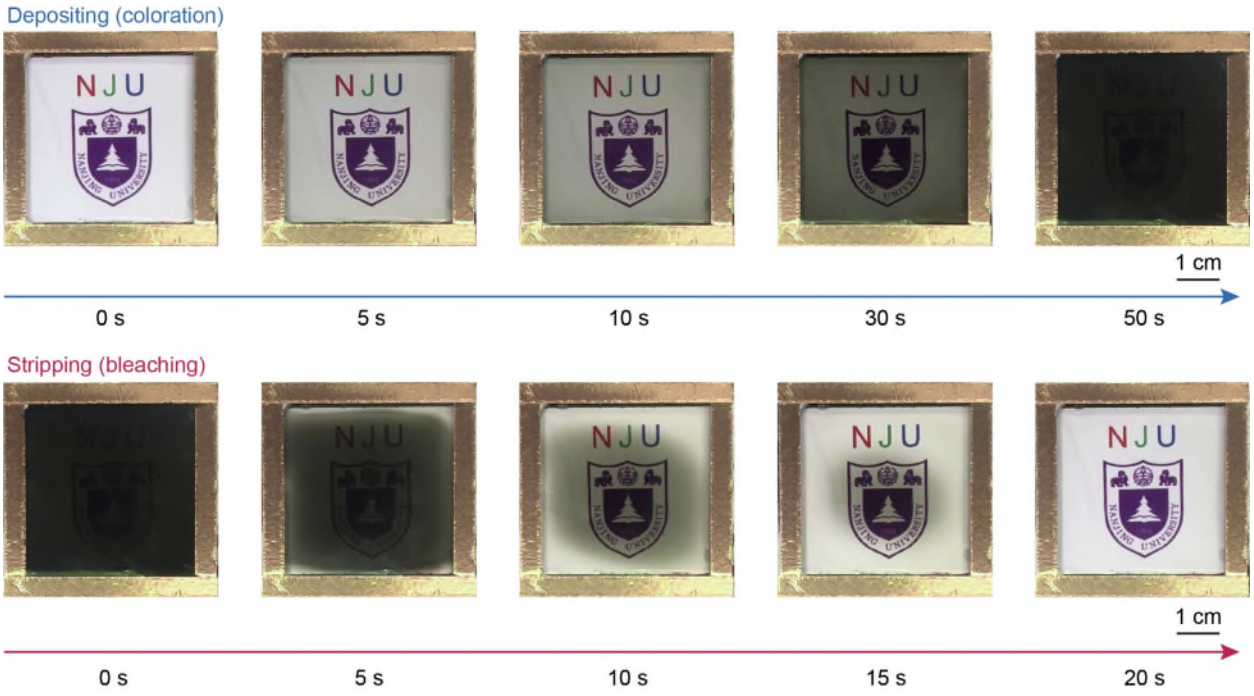

Figure R2. Optical photographs of the Cu–Bi film depositing (coloration) and stripping (bleaching) processes in a 25 cm^2 STDEC window.

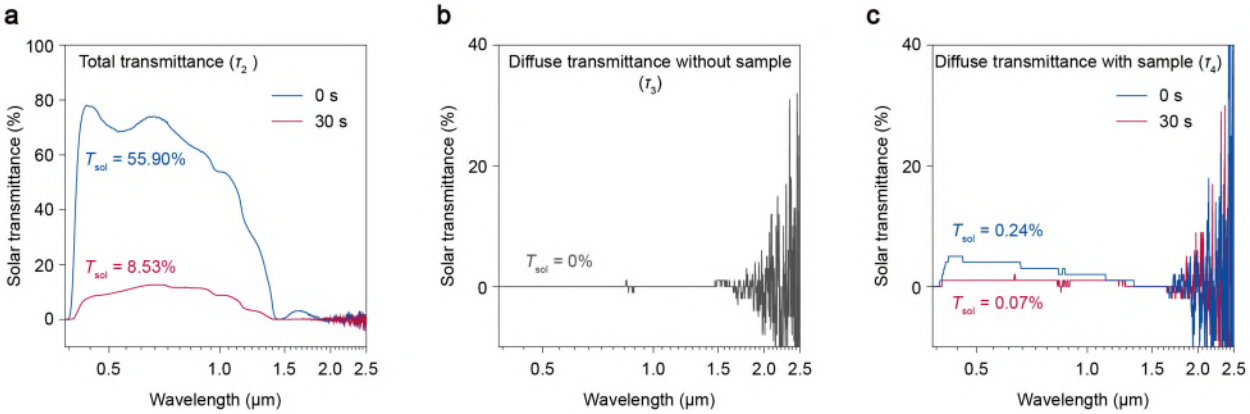

Figure R21. Haze calculation of the STDEC window. **a**, Total transmittance spectra of the STDEC window in the stripping and depositing states. **b**, Diffuse transmittance spectrum measured without the window sample. **c**, Diffuse transmittance spectra of the STDEC window in the stripping and depositing states.

Table R1. Haze calculation of the STDEC window.

STDEC sample	τ_1 (%)	τ_2 (%)	τ_3 (%)	τ_4 (%)	Haze (%)
Stripping state	100	55.90	0	0.24	0.43
Depositing state	100	8.53	0	0.07	0.82

[Changes in revised manuscript]:

We have made one main change in the revised manuscript and SI.

1. Page 12 of the revised manuscript.

We revised a sentence to emphasize the low Haze of the STDEC window:

"*A neutral color transition (clear-to-grey-to-black) with low haze values (Supplementary Fig. 25 and Supplementary Table 3) that minimally distort the view through the windows is more beneficial.*

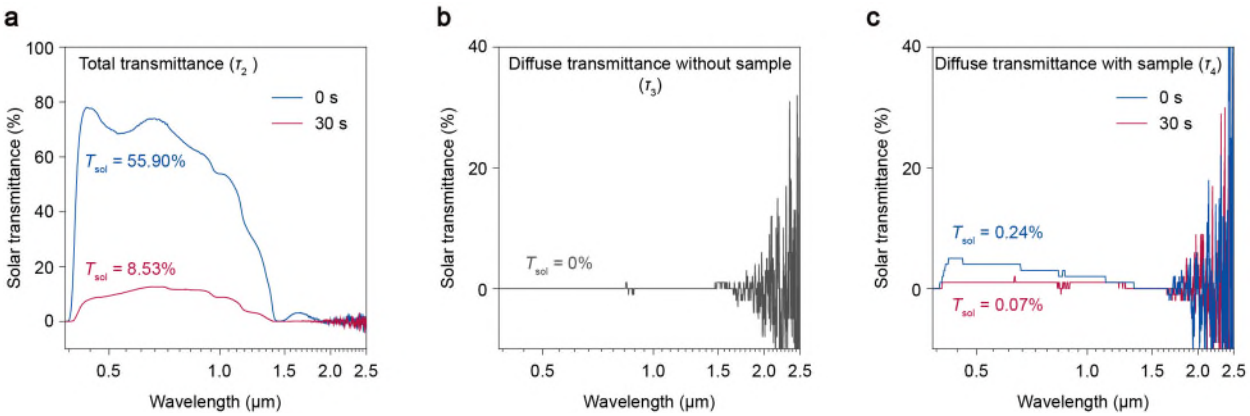

Supplementary Fig. 25: Haze calculation of the STDEC window. **a**, Total transmittance spectra of the STDEC window in the stripping and depositing states. **b**, Diffuse transmittance spectrum measured without the window sample. **c**, Diffuse transmittance spectra of the STDEC window in the stripping and depositing states.

Supplementary Table 3. Haze calculation of the STDEC window.

STDEC sample	τ_1 (%)	τ_2 (%)	τ_3 (%)	τ_4 (%)	Haze (%)
Stripping state	100	55.90	0	0.24	0.43
Depositing state	100	8.53	0	0.07	0.82

Note: To quantitatively assess the optical clarity of the window, we calculated the Haze in both the stripping and depositing states using the following formula:

$$\text{Haze (\%)} = \left[\left(\tau_4 / \tau_2 \right) - \tau_3 \left(\tau_2 / \tau_1 \right) \right] \times 100$$

where τ_1 is the total transmittance without the sample (100%); τ_2 is the total transmittance with the sample; τ_3 is the diffuse transmittance without the sample; and τ_4 is the diffuse transmittance with the sample. Supplementary Figure 25 presents the total and diffuse transmittance spectra of the STDEC window in the stripping and depositing states, along with the diffuse transmittance spectrum measured without the window sample. All spectra were obtained using an integrating sphere. There is nearly no diffuse transmittance across the solar spectrum, which explains the low measured haze values (Haze = 0.43% at T_{sol} = 55.90%; Haze = 0.82% at T_{sol} = 8.53%; Supplementary Table 3) and demonstrates the excellent optical clarity of the STDEC windows."

[Comment 5]: The building energy-saving simulation indicates an annual HVAC energy savings of up to 80 MJ/m² in extreme climate zones. Did the simulation account for the manufacturing costs, service life, and maintenance costs of the STDEC windows?

[Response]: We thank the reviewer for this insightful comment. The reported energy savings of up to 80 MJ m^{-2} yr^{-1} in extreme climate zones refer exclusively to operational energy performance and do not account for manufacturing costs, service life, or maintenance costs. We agree that these factors are critical for a comprehensive techno-economic assessment (TEA) of STDEC windows for real-world applications. Following the reviewer's suggestion, we conducted a detailed TEA analysis that includes all these factors.

(i) Cost analysis of the whole device

As summarized in **Tables R2–R4**, the manufacturing cost of the STDEC window is about **$6.38** per square meter of window area. Based on our building simulation model with a total window area of 652.62 m^2 and a total building area of 4982.19 m^2, this equates to approximately $0.84 per square meter of building area.

To contextualize this cost in terms of energy consumption, we converted it into an equivalent energy metric based on the electricity cost of $0.1745 per kWh, as reported by the U.S. Energy Information Administration (EIA). This manufacturing cost corresponds to an energy equivalent of **17.33 MJ m^{-2}** of building area.

Table R2. Cost analysis of electrolyte components.

Chemical's name	Price (US $/gram)
PVA	0.0022
$CuCl_2$	0.006
$BiCl_3$	0.0017
HCl	0.0011
LiBr	0.0014
Water	0.00084

Table R3. Cost analysis of device materials.

Material	Price (US $)
Glass	1.50/m^2 (Alibaba)
ITO	1.02/gram (Qinbangxc)
Cu mesh	3.76/m^2 (TWP)
PE	0.057/m^2 (Amazon)
3-nm-thick Pt	0.12/m^2 (Alibaba)
Butyl rubber tape	0.0047/gram (Alibaba)

Table R4. Cost analysis of the whole device.

Component	Price (US $/$m^2$)
Electrolyte	1.9
Cu mesh	0.15
ITO/Glass/ITO	4.07
3-nm-thick Pt	0.12
PE	0.057
Butyl rubber tape	0.086
Device	**6.38**

(ii) Service life

As reported in our work, the STDEC window demonstrates excellent cycling stability over 2,000 cycles, with only 1% degradation in optical contrast. At a typical operational frequency of two switching cycles per day for smart windows, this corresponds to approximately 2.7 years of service. If we then assume a steady degradation rate of 1% per year, the optical contrast would decline to 80% of its initial value after another 19 years, which we conservatively define as the end of lifetime. Therefore, the total estimated service life is ~21.7 years, which exceeds the 20-year service life for commercial smart windows.

The manufacturing cost (equivalent to 17.33 MJ/m^2 of building area), when amortized over the service life, corresponds to an annualized energy equivalent of only about **0.80 MJ m^{-2} yr^{-1}**.

(iii) Maintenance cost

The maintenance cost is dominated by the electricity consumption during switching. As reported in our work, the average electricity usage per square meter of building area of the STDEC window is 263.29 J m^{-2}. At a typical operational frequency of two switching cycles per day, the yearly electrical energy usage is about **0.19 MJ m^{-2} yr^{-1}**.

In summary, the total annualized energy usage accounting for manufacturing costs, service life, and maintenance costs of the STDEC window is calculated to **0.99 MJ m^{-2} yr^{-1}**. This value is nearly two orders of magnitude lower than the simulated annual HVAC energy savings (up to 80 MJ m^{-2} yr^{-1}), confirming the excellent energy-efficient performance of the STDEC window.

[Changes in revised manuscript]:

We have made two main changes in the revised manuscript and SI.

1. Page 16–17 of the revised manuscript.

We revised the sentence to emphasize the excellent energy-efficient performance of the STDEC windows even when accounting for the techno-economic assessment:

"*Cities with extreme hot and cold climates (Fig. 4c), such as Bangkok, Abu Dhabi, and Churchill, experienced the highest energy savings (over 80 MJ/m^2 even when accounting for the techno-economic assessment of the STDEC windows; Supplementary Note 4) compared to cities with more variable weather, such as Nanjing (30.8 MJ/m^2) and Santiago (27.7 MJ/m^2).*"

2. Page 62–64 of the revised SI.

We added a supplementary note to highlight the techno-economic assessment (TEA) analysis of the STDEC windows:

"***Supplementary Note 4. Techno-economic assessment (TEA) analysis of the STDEC window.***

To assess the energy-saving performance of the STDEC window for real-world applications, we conducted a comprehensive techno-economic assessment (TEA) accounting for manufacturing costs, service life, or maintenance costs.

(i) Cost analysis of the whole device

As summarized in Supplementary Tables 9–11, the manufacturing cost of the STDEC window is about $6.38 per square meter of window area. Based on our building simulation model with a total window area of 652.62 m^2 and a total building area of 4982.19 m^2, this equates to approximately $0.84 per square meter of building area.

To contextualize this cost in terms of energy consumption, we converted it into an equivalent energy metric based on the electricity cost of $0.1745 per kWh, as reported by the U.S. Energy Information Administration (EIA). This manufacturing cost corresponds to an energy equivalent of 17.33 MJ m^{-2} of building area.

Supplementary Table 9. Cost analysis of electrolyte components.

Chemical's name	Price (US $/gram)
PVA	0.0022
$CuCl_2$	0.006
$BiCl_3$	0.0017
HCl	0.0011
LiBr	0.0014
Water	0.00084

Supplementary Table 10. Cost analysis of device materials.

Material	Price (US $)
Glass	1.50/m^2 (Alibaba)
ITO	1.02/gram (Qinbangxc)
Cu mesh	3.76/m^2 (TWP)
PE	0.057/m^2 (Amazon)
3-nm-thick Pt	0.12/m^2 (Alibaba)
Butyl rubber tape	0.0047/gram (Alibaba)

Supplementary Table 11. Cost analysis of the whole device.

Component	Price (US $/m^2)
Electrolyte	1.9
Cu mesh	0.15
ITO/Glass/ITO	4.07
3-nm-thick Pt	0.12
PE	0.057
Butyl rubber tape	0.086
Device	**6.38**

(ii) Service life

As reported in our work, the STDEC window demonstrates excellent cycling stability over 2,000 cycles, with only 1% degradation in optical contrast. At a typical operational frequency of two switching cycles per day for smart windows, this corresponds to approximately 2.7 years of service. If we then assume a steady degradation rate of 1% per year, the optical contrast would decline to 80% of its initial value after another 19 years, which we conservatively define as the end of lifetime. Therefore, the total estimated service life is ~21.7 years, which exceeds the 20-year service life for commercial smart windows.

The manufacturing cost (equivalent to 17.33 MJ/m^2 of building area), when amortized over the service life, corresponds to an annualized energy equivalent of only about 0.80 MJ m^{-2} yr^{-1}.

(iii) Maintenance cost

The maintenance cost is dominated by the electricity consumption during switching. As reported in our work, the average electricity usage per square meter of building area of the STDEC window is 263.29 J m^{-2}. At a typical operational frequency of two switching cycles per day, the yearly electrical energy usage is about 0.19 MJ m^{-2} yr^{-1}.

In summary, the total annualized energy usage accounting for manufacturing costs, service life, and maintenance costs of the STDEC window is calculated to 0.99 MJ m^{-2} yr^{-1}. This value is nearly two orders of magnitude lower than the simulated annual HVAC energy savings (up to 80 MJ m^{-2} yr^{-1}), confirming the excellent energy-efficient performance of the STDEC window."

[Comment 6]: In addition, the solar heat gain coefficient is an important parameter to evaluate a window, especially for an EC window. However, such fundamental data on the STDEC device is missing. Additionally, the energy simulations appear to assume an identical U-value for all window configurations; The authors should address this.

[Response]: We thank the reviewer for this constructive suggestion. We have measured the solar heat gain coefficient (SHGC) and *U*-value using outdoor thermal measurements. The measurement and calculation details are as follows.

The solar heat gain coefficient (SHGC) is defined as:

$$\mathrm{SHGC} = \left(T_{\mathrm{sol}} + \frac{U}{h_{\mathrm{o}}} A_{\mathrm{sol}} \right)$$

where T_{sol} is the solar transmittance;

A_{sol} is the solar absorbance;

h_{o} is the outdoor surface heat transfer coefficient, h_{o} = 8.0 W m^{-2} K^{-1} (refer to ISO-15099-2003);

U is the universal heat transfer coefficient, which can be given by:

$$U = \frac{1}{\frac{1}{h_{\mathrm{conv,o}} + h_{\mathrm{rad,o}}} + \frac{1}{h_{\mathrm{conv,i}} + h_{\mathrm{rad,i}}} + \frac{L_{\mathrm{device}}}{k_{\mathrm{device}}}}$$

where $h_{\mathrm{conv,\,o}}$ is the outdoor convective heat transfer coefficient, $h_{\mathrm{conv,\,o}}$ = 8.0 W m^{-2} K^{-1};

$h_{\mathrm{conv,\,i}}$ is the indoor convective heat transfer coefficient, $h_{\mathrm{conv,\,i}}$ = 3.6 W m^{-2} K^{-1};

$h_{\mathrm{rad,\,o}}$ is the outdoor radiative heat transfer coefficient;

$h_{\mathrm{rad,\,i}}$ is the indoor radiative heat transfer coefficient;

k_{device} and L_{device} are the thermal conductivity and thickness of the window device.

The outdoor convective heat transfer coefficient ($h_{\mathrm{rad,\,o}}$) can be calculated as:

$$h_{\mathrm{rad,o}} = \frac{\varepsilon_{\mathrm{device,o}} \sigma \left(T_{\mathrm{device,o}}^4 - T_{\mathrm{rm,o}}^4 \right)}{T_{\mathrm{device,o}} - T_{\mathrm{rm,o}}} = \varepsilon_{\mathrm{device,o}} \sigma \left(T_{\mathrm{device,o}}^2 + T_{\mathrm{rm,o}}^2 \right) \left(T_{\mathrm{device,o}} + T_{\mathrm{rm,o}} \right)$$

where $\varepsilon_{\mathrm{device,\,o}}$ is the emissivity of the outside device surface;

σ is Stefan-Boltzmann constant, 5.67 × 10^{-8} W m^{-2} K^{-4};

$T_{\mathrm{device,\,o}}$ is the temperature of the outside device surface;

$T_{\mathrm{rm,\,o}}$ is the mean radiative temperature of outside ambient, which can be expressed as:

$$T_{\mathrm{rm,o}} = \left(\frac{\left(F_{\mathrm{gd}} + \left(1 - f_{\mathrm{clr}}\right) F_{\mathrm{sky}}\right)\sigma T_{\mathrm{ex}}^4 + f_{\mathrm{clr}} F_{\mathrm{sky}} J_{\mathrm{sky}}}{\sigma} \right)^{1/4}$$

$$F_{\mathrm{gd}} = 1 - F_{\mathrm{sky}}$$

$$F_{\mathrm{sky}} = \frac{1 + \cos\phi}{2}$$

$$J_{\mathrm{sky}} = 5.31 \times 10^{-13} T_{\mathrm{air}}^6$$

where F_{gd} and F_{sky} are the view factors from the outside glass surface to the ground and sky, respectively;

f_{clr} is the fraction of the sky that is clear;

T_{ex} is the external air temperature;

Φ is the tilt angle of the glass;

J_{sky} is the radiosity of clear sky;

T_{air} is the dry bulb temperature.

For a horizontal window ($F_{\mathrm{sky}} = 1, F_{\mathrm{gd}} = 0, f_{\mathrm{clr}} = 1$):

$$T_{\mathrm{rm,o}} = \left(\frac{J_{\mathrm{sky}}}{\sigma} \right)^{1/4}$$

The indoor radiative heat transfer coefficient ($h_{\mathrm{rad,\,i}}$) can be determined by:

$$h_{\mathrm{rad,i}} = \frac{\varepsilon_{\mathrm{device,i}}\sigma\left(T_{\mathrm{device,i}}^4 - T_{\mathrm{rm,i}}^4\right)}{T_{\mathrm{device,i}} - T_{\mathrm{rm,i}}} = \frac{\varepsilon_{\mathrm{device,i}}\sigma\left(T_{\mathrm{device,i}}^4 - T_{\mathrm{int}}^4\right)}{T_{\mathrm{device,i}} - T_{\mathrm{int}}} = \varepsilon_{\mathrm{device,i}}\sigma\left(T_{\mathrm{device,i}}^2 + T_{\mathrm{int}}^2\right)\left(T_{\mathrm{device,i}} + T_{\mathrm{int}}\right)$$

where $\varepsilon_{\mathrm{device,\,i}}$ is the emissivity of the inside device surface;

σ is Stefan-Boltzmann constant, 5.67×10^{-8} W m^{-2} K^{-4};

$T_{\mathrm{device,\,i}}$ is the temperature of the inside device surface;

$T_{\mathrm{rm,\,i}} = T_{\mathrm{int}}$ is the internal air temperature.

Table R5 presents the temperatures recorded from outdoor thermal measurements required for the calculation. Based on these data and the optical properties of the windows (**Table R6)**, we calculated the *U*-values and SHGC for the STDEC window and the control windows (normal glass, low-E glass, and EC window). Among all the windows tested, the STDEC window has the lowest *U*-value and the largest dynamic SHGC modulation range between the heating and cooling modes, highlighting its excellent optical and thermal regulation capability.

Table R5. Outdoor temperature measurement conducted at a dry bulb temperature of T_{air} = 298 K.

Temperature (K)	EC window (heating mode)	EC window (cooling mode)	STDEC window (heating mode)	STDEC window (cooling mode)
Outside surface ($T_{device,\ o}$)	315	319	316	318
Inside surface ($T_{device,\ i}$)	320	323	320	319
Internal air (T_{int})	325	314	323	310

Table R6. Optical and thermal properties for window samples used in building energy simulation.

Optical properties	Normal glass	Low-E glass	EC window (heating mode)	EC window (cooling mode)	STDEC window (heating mode)	STDEC window (cooling mode)
T_{vis} (%)	88.1	85.0	67.2	0.04	64.8	0.04
$R_{vis\text{-}Front}$ (%)	8.0	5.6	11.2	10.3	15.0	16.0
$R_{vis\text{-}Back}$ (%)	8.0	7.9	10.8	25.5	14.9	16.5
T_{sol} (%)	77.5	63.0	53.3	0.06	52.2	0.06
$R_{sol\text{-}Front}$ (%)	7.1	19.0	9.6	8.2	17.8	15.7
$R_{sol\text{-}Back}$ (%)	7.1	22.0	16.5	33.8	11.4	20.2
$\varepsilon_{LWIR\text{-}Front}$	0.84	0.84	0.84	0.84	0.08	0.95
$\varepsilon_{LWIR\text{-}Back}$	0.84	0.1	0.84	0.84	0.95	0.08
U-value (W m^{-2} K^{-1})	**5.8**	**5.7**	**5.5**	**5.5**	**4.6**	**3.2**
SHGC	**0.89**	**0.76**	**0.79**	**0.69**	**0.69**	**0.40**

Moreover, we revised the building energy-saving simulation using the different *U*-values from **Table R6** for all window configurations. The updated results are shown in **Figures R22–26** and **Table R7**.

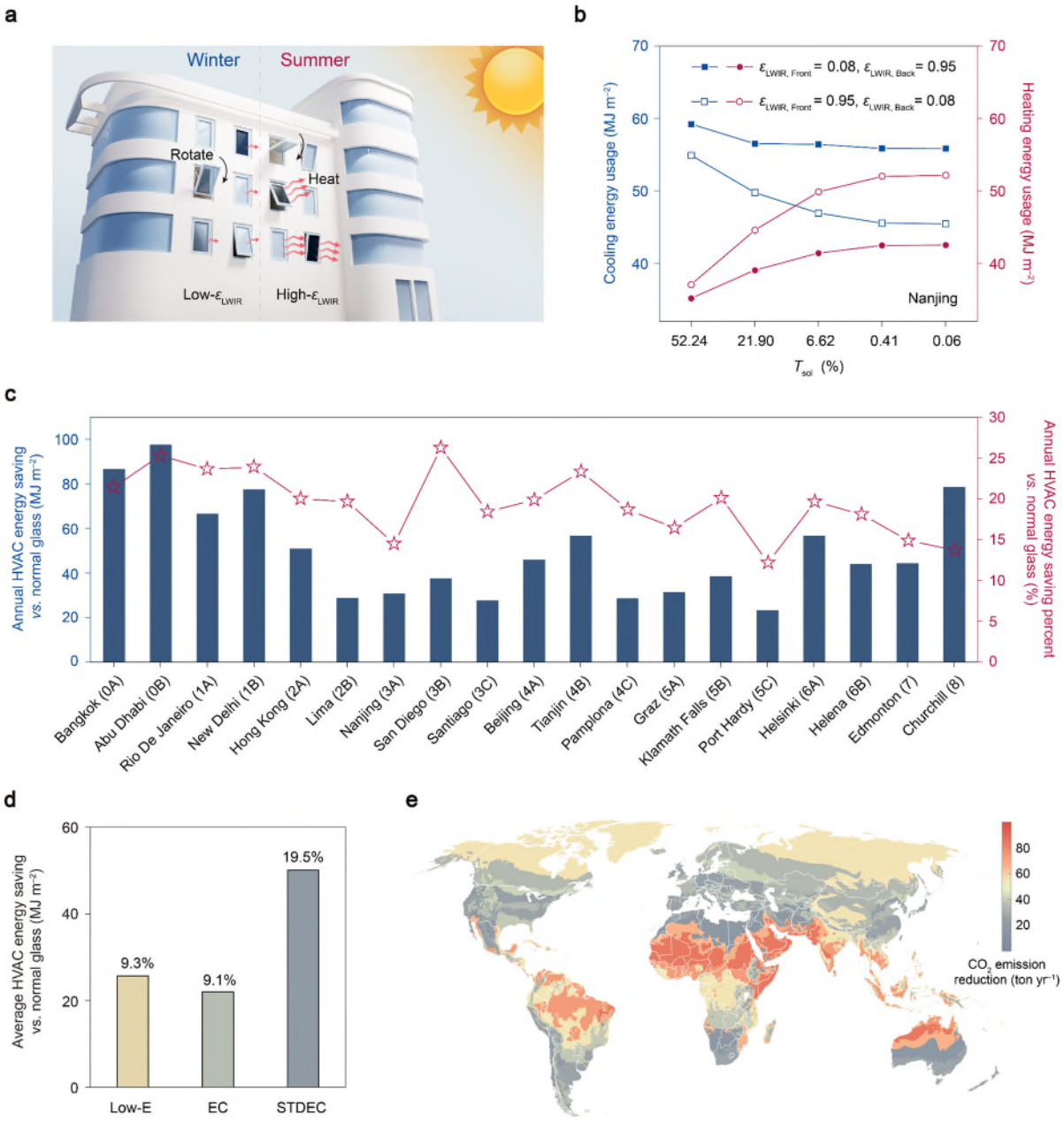

Figure R22. Simulated all-season energy savings and CO_2 emission reductions for window applications. **a**, Schematic of a building with the rotational STDEC window for thermal regulation. **b**, The heating and cooling energy consumption of a medium office building in Nanjing enveloped with low- or high-emissivity windows at various optical states. **c**, Annual operational HVAC energy savings and saving percentage of buildings with the STDEC window for 19 typical cities in different climate zones. **d**, Average HVAC energy savings in buildings with STDEC, EC, and low-E windows, in contrast to those using the normal glass. **e**, Yearly CO_2 emission reductions of a medium office building using the STDEC window in different global climate zones.

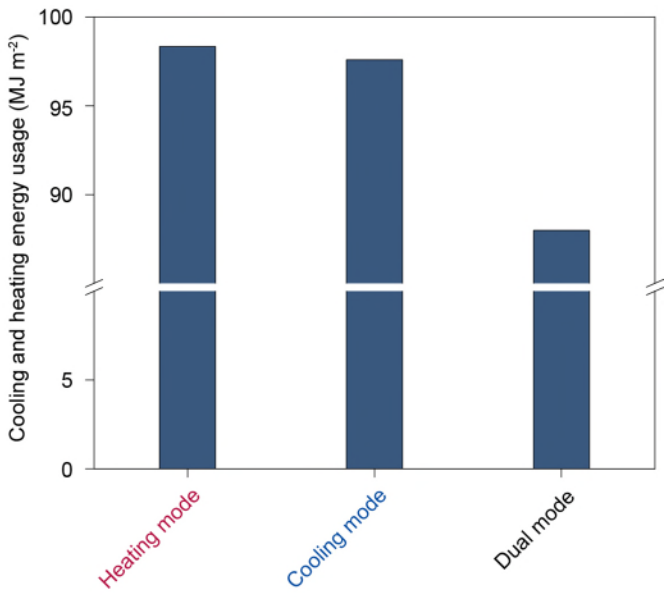

Figure R23. Comparison of cooling and heating energy usage using static emissivity window samples and dynamic emissivity window samples (i.e., STDEC windows). The static emissivity window samples have a constant emissivity of 0.08 (heating mode) or 0.95 (cooling mode) for heating and cooling, whereas the STDEC windows have variable emissivity values for heating and cooling, with a value of 0.08 for heating and 0.95 for cooling.

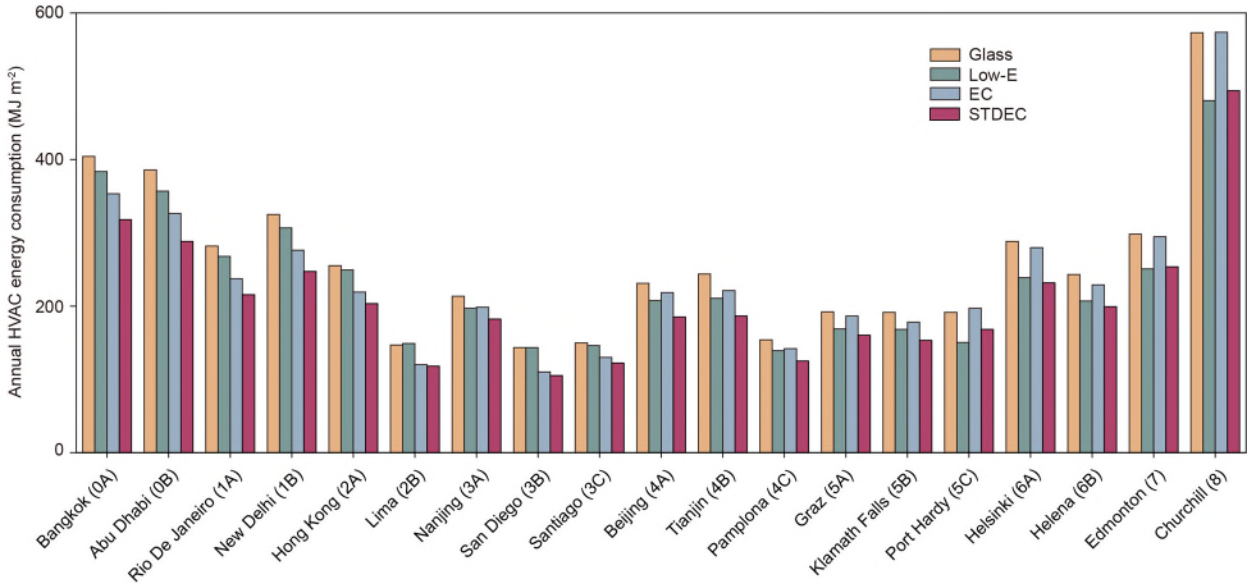

Figure R24. Annual HVAC energy consumption for four different window samples (i.e., normal glass, low-E glass, EC window, and STDEC window) across 19 representative cities in various climate zones.

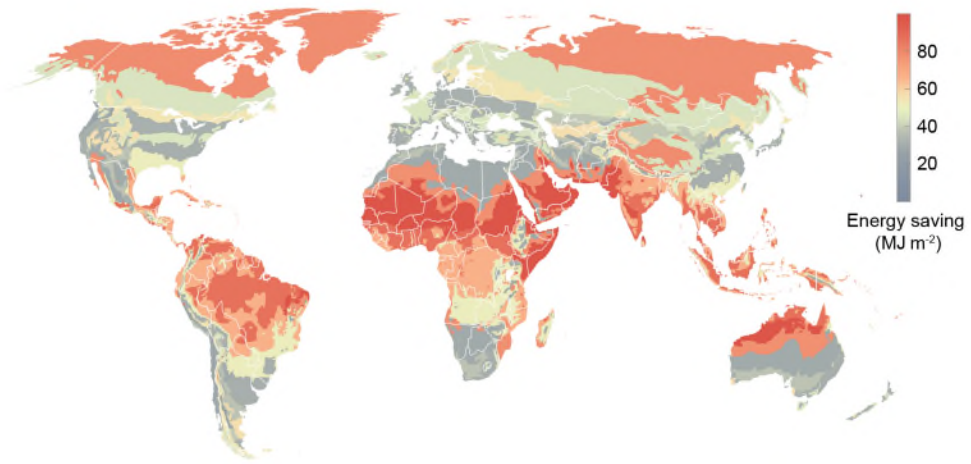

Figure R25. Year-round HVAC energy-saving map of the STDEC window in various global climate zones, using a normal glass as the baseline.

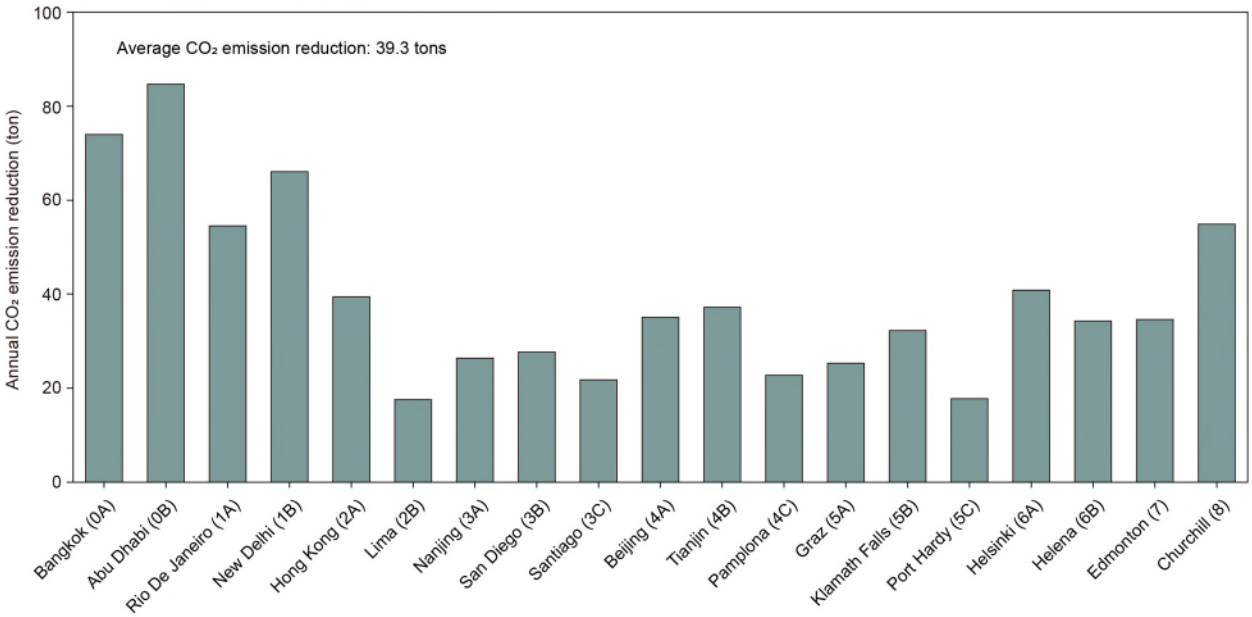

Figure R26. Annual CO_2 emission reductions of a medium office building with STDEC windows in 19 representative cities of different climate zones, with an average reduction of 39.3 tons compared with the normal glass baseline.

Table R7. Annual CO_2 emission reductions of a medium office building with STDEC windows in 19 representative cities of different climate zones.

Region	Thermal zone	Thermal climate zone name	Annual CO_2 emission reduction (ton)
Bangkok, Thailand	0A	Extremely Hot Humid	74.0
Abu Dhabi, United Arab Emirates	0B	Extremely Hot Dry	84.7
Rio De Janeiro, Brazil	1A	Very Hot Humid	54.5
New Delhi, India	1B	Very Hot Dry	66.1
Hong Kong, China	2A	Hot Humid	39.4
Lima, Peru	2B	Hot Dry	17.5
Nanjing, China	3A	Warm Humid	26.4
San Diego, USA	3B	Warm Dry	27.7
Santiago, Chile	3C	Warm Marine	21.8
Beijing, China	4A	Mixed Humid	35.1
Tianjin, China	4B	Mixed Dry	37.2
Pamplona, Spain	4C	Mixed Marine	22.7
Graz, Austria	5A	Cool Humid	25.3
Klamath Falls, USA	5B	Cool Dry	32.3
Port Hardy, Canada	5C	Cool Marine	17.8
Helsinki, Finland	6A	Cold Humid	40.9
Helena, USA,	6B	Cold Dry	34.3
Edmonton, Canada	7	Very Cold	34.6
Churchill, Canada	8	Subarctic/Arctic	54.9

[Changes in revised manuscript]:

We have made three main changes in the revised manuscript and SI.

1. Page 4–5 of the revised manuscript.

We revised the sentence to highlight the updated results of building energy-saving simulation:

"*Our building energy calculations indicate that the STDEC window demonstrates an average HVAC energy saving of 19.5% across all global climate zones, outperforming commercial low-emissivity (low-E) glass windows (9.3%) and standard RME-based EC windows (9.1%).*"

2. Page 16–19 of the revised manuscript.

We revised the "**Energy-saving building application**" section to highlight the updated results of building energy-saving simulation:

"***Energy-saving building application***

To evaluate the energy-saving efficacy of the STDEC window and its potential to reduce carbon dioxide (CO_2) emissions, we performed energy simulations for building application (Fig. 4a). We investigated the year-round heating and cooling energy consumption (Fig. 4b) in a reference medium office building model (total floor area of 4982.19 m^2 and window-to-wall ratio of 33% as illustrated in Supplementary Fig. 41) with low-/high-emissivity and varied T_{sol} windows, utilizing EnergyPlus. This calculation suggests that the yearly cooling energy consumption is clearly lower with high-emissivity windows (represented by the blue blank frame in Fig. 4b) than with low-emissivity ones, especially at low T_{sol} conditions. In contrast, the annual heating energy usage is greatly reduced when using low-emissivity windows (shown by the solid red dot in Fig. 4b) compared to high-emissivity windows. By spatially rotating the window to alter its emissivity (with ε_{LWIR} of 0.08 for heating and ε_{LWIR} of 0.95 for cooling), the STDEC window located in Nanjing can save up to 10 MJ/m^2 energy usage per year compared with the static emissivity windows (Supplementary Fig. 42).

To determine the most effective use of the STDEC window, we then examined its energy-saving performance on a global scale, concentrating on 19 cities that encompass all climate zones. The reference medium office building with normal glass windows was established as the baseline for our analysis, after which we modified the optical and thermal properties of the windows, in accordance with our measurements detailed in Supplementary Table 6. We compared the annual HVAC energy consumption of a building fitted with the STDEC window with that of buildings featuring the normal glass, low-E glass, and RME-based EC window. The findings indicate that

buildings with STDEC windows have considerably reduced year-round HVAC energy consumption compared to those with normal glass windows (Supplementary Fig. 43). Supplementary Figure 44 presents a color map that shows the yearly energy savings achieved by using the STDEC windows for heating and cooling in a medium office building across various cities worldwide. Cities with extreme hot and cold climates (Fig. 4c), such as Bangkok, Abu Dhabi, and Churchill, experienced the highest energy savings (over 80 MJ/m^2 even when accounting for the techno-economic assessment of the STDEC windows; Supplementary Note 4) compared to cities with more variable weather, such as Nanjing (30.8 MJ/m^2) and Santiago (27.7 MJ/m^2). Notably, many cities in subtropical and temperate zones, despite experiencing considerable weather and seasonal fluctuations, can still achieve an annual HVAC energy saving percentage of about 20.2% (Fig. 4c). Globally, the average year-round energy conservation for building HVAC systems using the STDEC window can reach 19.5% (Fig. 4d), substantially surpassing the 9.3% savings from commercial low-E glass and the 9.1% from RME-based EC windows. The calculation results indicate that the STDEC window, which adapts to the changing weather conditions, can provide higher energy benefits across all climate zones around the world.

To further illustrate the positive impact of the STDEC window on sustainability in building operations, we computed the equivalent CO_2 emission reductions that resulted from the annual energy savings. More details about the CO_2 emission reductions for the 19 selected cities worldwide are available in Supplementary Table 7. The CO_2 emission reduction map (Fig. 4e) also highlighted the increased potential of the STDEC window in very hot and cold areas. Applying the STDEC window in the reference medium office building resulted in an average annual decrease of 39.3 tons of CO_2 emissions compared with the baseline (Supplementary Fig. 45).

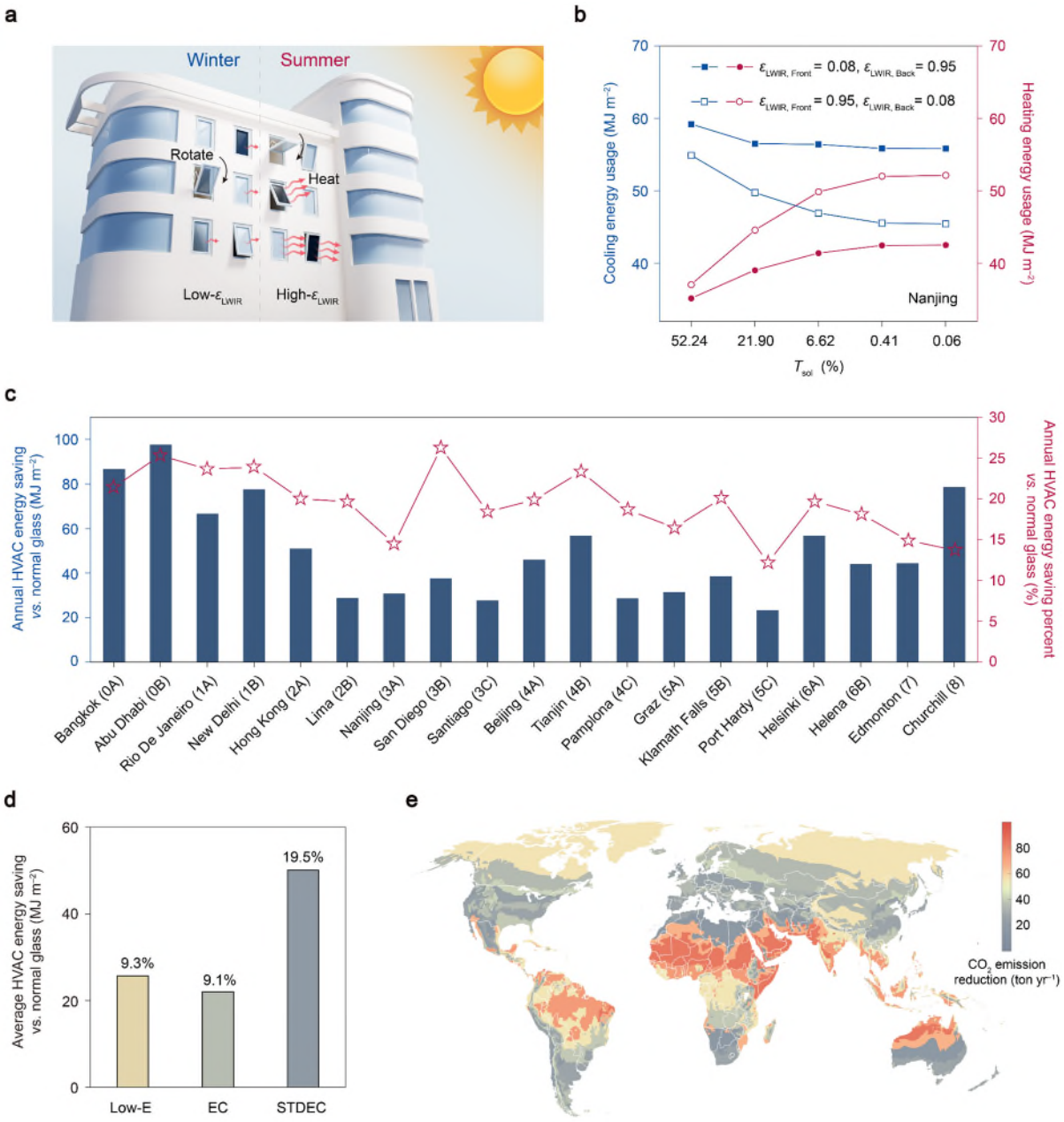

Fig. 4 | Simulated all-season energy savings and CO_2 emission reductions for window applications. a, Schematic of a building with the rotational STDEC window for thermal regulation. **b**, The heating and cooling energy consumption of a medium office building in Nanjing enveloped with low- or high-emissivity windows at various optical states. **c**, Annual operational HVAC energy savings and saving percentage of buildings with the STDEC window for 19 typical cities in different climate zones. **d**, Average HVAC energy savings in buildings with STDEC, EC, and low-E windows, in contrast to those using the normal glass. **e**, Yearly CO_2 emission reductions of a medium office building using the STDEC window in different global climate zones.

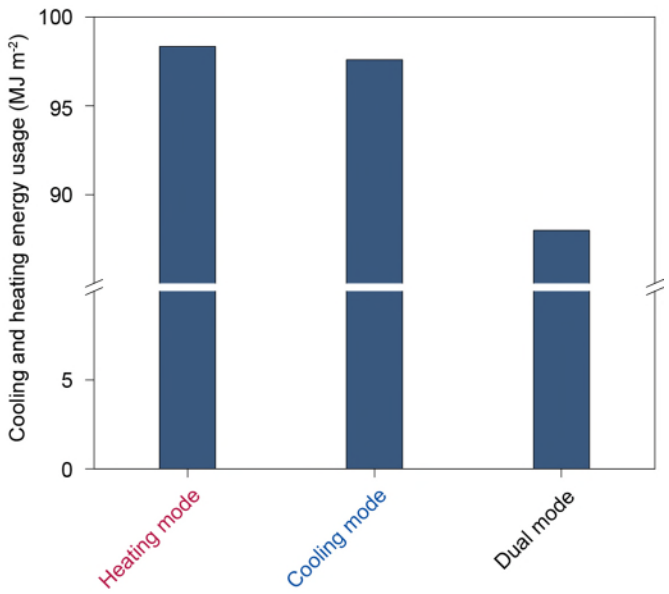

Supplementary Fig. 42: Comparison of cooling and heating energy usage using static emissivity window samples and dynamic emissivity window samples (i.e., STDEC windows). The static emissivity window samples have a constant emissivity of 0.08 (heating mode) or 0.95 (cooling mode) for heating and cooling, whereas the STDEC windows have variable emissivity values for heating and cooling, with a value of 0.08 for heating and 0.95 for cooling.

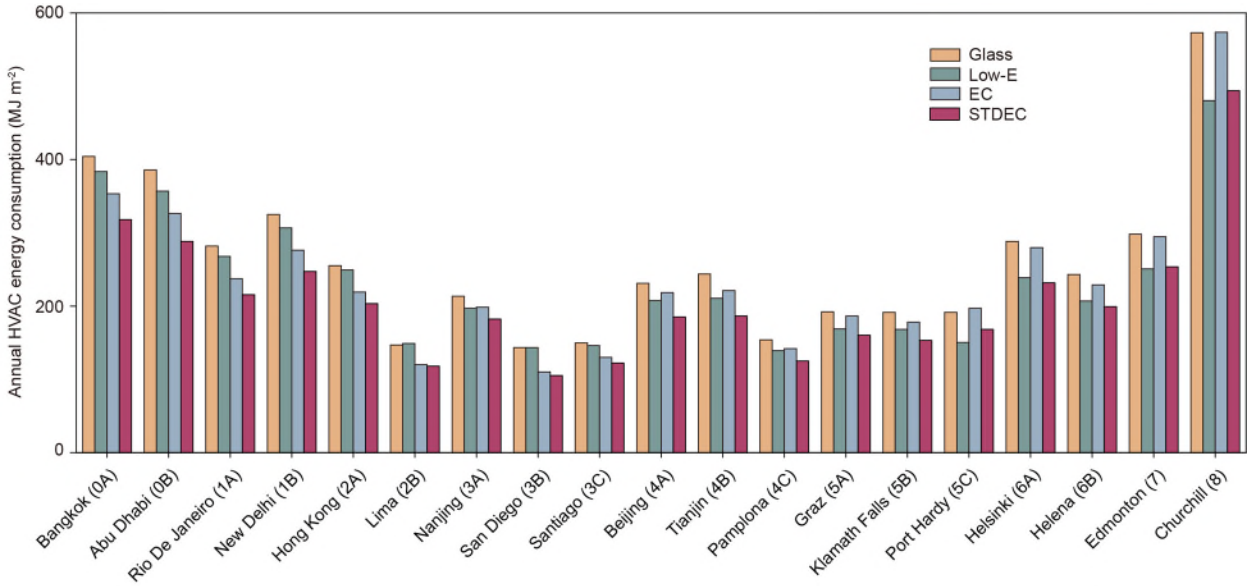

Supplementary Fig. 43: Annual HVAC energy consumption for four different window samples (i.e., normal glass, low-E glass, EC window, and STDEC window) across 19 representative cities in various climate zones.

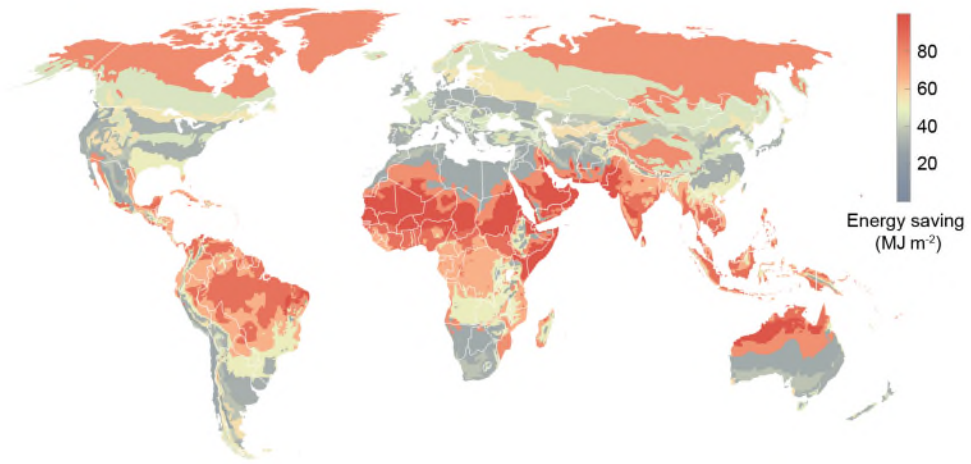

Supplementary Fig. 44: Year-round HVAC energy-saving map of the STDEC window in various global climate zones, using a normal glass as the baseline.

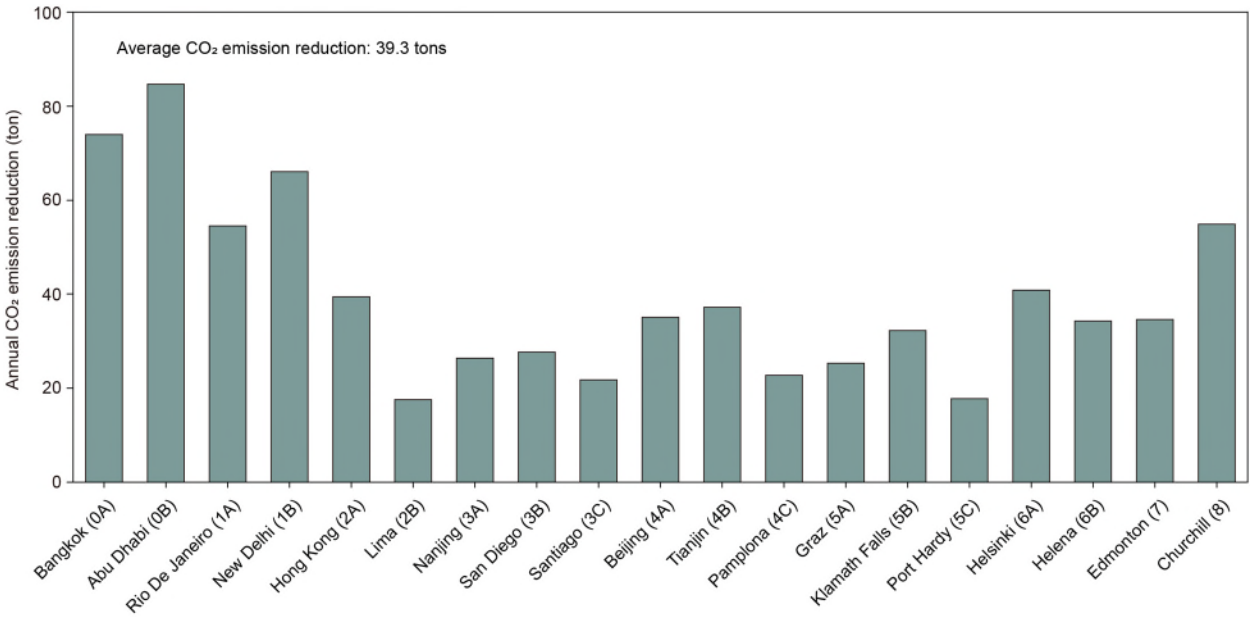

Supplementary Fig. 45: Annual CO_2 emission reductions of a medium office building with STDEC windows in 19 representative cities of different climate zones, with an average reduction of 39.3 tons compared with the normal glass baseline.

Supplementary Table 6. Optical and thermal properties for window samples used in building energy simulation.

Optical properties	Normal glass	Low-E glass	EC window (heating mode)	EC window (cooling mode)	STDEC window (heating mode)	STDEC window (cooling mode)
T_{vis} (%)	88.1	85.0	67.2	0.04	64.8	0.04
$R_{vis\text{-}Front}$ (%)	8.0	5.6	11.2	10.3	15.0	16.0
$R_{vis\text{-}Back}$ (%)	8.0	7.9	10.8	25.5	14.9	16.5
T_{sol} (%)	77.5	63.0	53.3	0.06	52.2	0.06
$R_{sol\text{-}Front}$ (%)	7.1	19.0	9.6	8.2	17.8	15.7
$R_{sol\text{-}Back}$ (%)	7.1	22.0	16.5	33.8	11.4	20.2
$\varepsilon_{LWIR\text{-}Front}$	0.84	0.84	0.84	0.84	0.08	0.95
$\varepsilon_{LWIR\text{-}Back}$	0.84	0.1	0.84	0.84	0.95	0.08
U-value (W m^{-2} K^{-1})	5.8	5.7	5.5	5.5	4.6	3.2
SHGC	0.89	0.76	0.79	0.69	0.69	0.40

Supplementary Table 7. Annual CO_2 emission reductions of a medium office building with STDEC windows in 19 representative cities of different climate zones.

Region	Thermal zone	Thermal climate zone name	Annual CO_2 emission reduction (ton)
Bangkok, Thailand	0A	Extremely Hot Humid	74.0
Abu Dhabi, United Arab Emirates	0B	Extremely Hot Dry	84.7
Rio De Janeiro, Brazil	1A	Very Hot Humid	54.5
New Delhi, India	1B	Very Hot Dry	66.1
Hong Kong, China	2A	Hot Humid	39.4
Lima, Peru	2B	Hot Dry	17.5
Nanjing, China	3A	Warm Humid	26.4
San Diego, USA	3B	Warm Dry	27.7
Santiago, Chile	3C	Warm Marine	21.8
Beijing, China	4A	Mixed Humid	35.1
Tianjin, China	4B	Mixed Dry	37.2
Pamplona, Spain	4C	Mixed Marine	22.7
Graz, Austria	5A	Cool Humid	25.3
Klamath Falls, USA	5B	Cool Dry	32.3
Port Hardy, Canada	5C	Cool Marine	17.8
Helsinki, Finland	6A	Cold Humid	40.9
Helena, USA,	6B	Cold Dry	34.3
Edmonton, Canada	7	Very Cold	34.6
Churchill, Canada	8	Subarctic/Arctic	54.9

”

3. Page 65–67 of the revised SI.

We added a supplementary note to emphasize the calculation of SHGC and *U*-value:

"***Supplementary Note 5. Calculation of SHGC and U-value for the windows.***

The solar heat gain coefficient (SHGC) is defined as:

$$\mathrm{SHGC} = \left(T_{\mathrm{sol}} + \frac{U}{h_{\mathrm{o}}} A_{\mathrm{sol}} \right)$$

where T_{sol} is the solar transmittance;

A_{sol} is the solar absorbance;

h_o is the outdoor surface heat transfer coefficient, h_o = 8.0 W m^{-2} K^{-1} (refer to ISO-15099-2003)[14]; U is the universal heat transfer coefficient, which can be given by:

$$U = \frac{1}{\frac{1}{h_{\mathrm{conv,o}} + h_{\mathrm{rad,o}}} + \frac{1}{h_{\mathrm{conv,i}} + h_{\mathrm{rad,i}}} + \frac{L_{\mathrm{device}}}{k_{\mathrm{device}}}}$$

where $h_{conv,\,o}$ is the outdoor convective heat transfer coefficient, $h_{conv,\,o}$ = 8.0 W m^{-2} K^{-1};

$h_{conv,\,i}$ is the indoor convective heat transfer coefficient, $h_{conv,\,i}$ = 3.6 W m^{-2} K^{-1};

$h_{rad,\,o}$ is the outdoor radiative heat transfer coefficient;

$h_{rad,\,i}$ is the indoor radiative heat transfer coefficient;

k_{device} and L_{device} are the thermal conductivity and thickness of the window device.

The outdoor convective heat transfer coefficient ($h_{rad,\,o}$) can be calculated as:

$$h_{\mathrm{rad,o}} = \frac{\varepsilon_{\mathrm{device,o}} \sigma \left(T_{\mathrm{device,o}}^4 - T_{\mathrm{rm,o}}^4 \right)}{T_{\mathrm{device,o}} - T_{\mathrm{rm,o}}} = \varepsilon_{\mathrm{device,o}} \sigma \left(T_{\mathrm{device,o}}^2 + T_{\mathrm{rm,o}}^2 \right) \left(T_{\mathrm{device,o}} + T_{\mathrm{rm,o}} \right)$$

where $\varepsilon_{device,\,o}$ is the emissivity of the outside device surface;

σ is Stefan-Boltzmann constant, 5.67 × 10^{-8} W m^{-2} K^{-4};

$T_{device,\,o}$ is the temperature of the outside device surface;

$T_{rm,\,o}$ is the mean radiative temperature of outside ambient, which can be expressed as:

$$T_{\mathrm{rm,o}} = \left(\frac{\left(F_{\mathrm{gd}} + \left(1 - f_{\mathrm{clr}} \right) F_{\mathrm{sky}} \right) \sigma T_{\mathrm{ex}}^4 + f_{\mathrm{clr}} F_{\mathrm{sky}} J_{\mathrm{sky}}}{\sigma} \right)^{1/4}$$

$$F_{\mathrm{gd}} = 1 - F_{\mathrm{sky}}$$

$$F_{\mathrm{sky}} = \frac{1 + \cos \phi}{2}$$

$$J_{\text{sky}} = 5.31\times10^{-13}T_{\text{air}}^{6}$$

where F_{gd} and F_{sky} are the view factors from the outside glass surface to the ground and sky, respectively;

f_{clr} is the fraction of the sky that is clear;

T_{ex} is the external air temperature;

Φ is the tilt angle of the glass;

J_{sky} is the radiosity of clear sky;

T_{air} is the dry bulb temperature.

For a horizontal window ($F_{sky} = 1, F_{gd} = 0, f_{clr} = 1$):

$$T_{\text{rm,o}} = \left(\frac{J_{\text{sky}}}{\sigma}\right)^{1/4}$$

The indoor radiative heat transfer coefficient ($h_{rad,\,i}$) can be determined by:

$$h_{\text{rad,i}} = \frac{\varepsilon_{\text{device,i}}\sigma\left(T_{\text{device,i}}^{4} - T_{\text{rm,i}}^{4}\right)}{T_{\text{device,i}} - T_{\text{rm,i}}} = \frac{\varepsilon_{\text{device,i}}\sigma\left(T_{\text{device,i}}^{4} - T_{\text{int}}^{4}\right)}{T_{\text{device,i}} - T_{\text{int}}} = \varepsilon_{\text{device,i}}\sigma\left(T_{\text{device,i}}^{2} + T_{\text{int}}^{2}\right)\left(T_{\text{device,i}} + T_{\text{int}}\right)$$

where $\varepsilon_{device,\,i}$ is the emissivity of the inside device surface;

σ is Stefan-Boltzmann constant, 5.67×10^{-8} W m^{-2} K^{-4};

$T_{device,\,i}$ is the temperature of the inside device surface;

$T_{rm,\,i} = T_{int}$ is the internal air temperature.

Supplementary Table 12 presents the temperatures recorded from outdoor thermal measurements required for the calculation. Based on these data and the optical properties of the windows (Supplementary Table 6), we calculated the U-values and SHGC for the STDEC window and the control windows (normal glass, low-E glass, and EC window). Among all the windows tested, the STDEC window has the lowest U-value and the largest dynamic SHGC modulation range between the heating and cooling modes, highlighting its excellent optical and thermal regulation capability.

Supplementary Table 12. Outdoor temperature measurement conducted at a dry bulb temperature of T_{air} = 298 K.

Temperature (K)	EC window (heating mode)	EC window (cooling mode)	STDEC window (heating mode)	STDEC window (cooling mode)
Outside surface ($T_{device,\ o}$)	315	319	316	318
Inside surface ($T_{device,\ i}$)	320	323	320	319
Internal air (T_{int})	325	314	323	310

"

[Comment 7]: While the optimized ITO layer of 185nm is needed, scaling the RME system to meter-scale architectural windows presents challenges regarding uniformity and switching kinetics. The authors should comment on how to maintain the same performance of a 100 cm² device across larger dimensions, typical of commercial windows.

[Response]: We thank the reviewer for this important comment. We agree that metre-scale device performance is critical for commercial window applications. The major challenge in scaling the STDEC window lies in minimizing the voltage drop across the transparent conductive electrode to achieve uniform deposition or coloration, similar to that of a 100 cm^2 device. The equation for voltage drops across a square electrode is given by:

$$\Delta V = -\left(JR_s/2\right)\left(L/2\right)^2$$

where J is the current density, R_s is the sheet resistance, and L is the electrode length. Several methods can achieve uniform deposition or coloration over large-area windows.

(**i**) One typical approach involves lowering the average current density (**Figure R7a**). With a 185-nm-thick ITO electrode (sheet resistance 8 Ω sq^{-1}) as reported in our work, the voltage drop across a 30 cm × 30 cm window is only –0.11 V (**Figure R7b**, red line). This is much lower than the applied voltage of –1.0 V, resulting in homogeneous deposition and coloration of the window **(Figure R7c**). However, scaling this architecture to metre-scale windows could still be challenging due to a large voltage drop over –1.0 V.

(**ii**) An alternative way to achieve fast and uniform coloration is to reduce the sheet resistance of the electrodes (**Figure R7b**, blue and orange lines). For example, employing a highly conductive metal mesh electrode, with a sheet resistance of 0.12 Ω sq^{-1} and 80% of optical transparency (*Adv.*

Mater. Technol. 2023, *8*, 2201406.), can reduce the voltage drop across a 4 m^2 metre-scale window to less than –0.1 V.

(**iii**) A final strategy bypasses the trade-off between voltage drop and window dimension through structural design. This can be achieved by designing the patterned electrode to shorten the current path or by combining smaller units into a modular large-area window, allowing for both uniform deposition/coloration and fast switching.

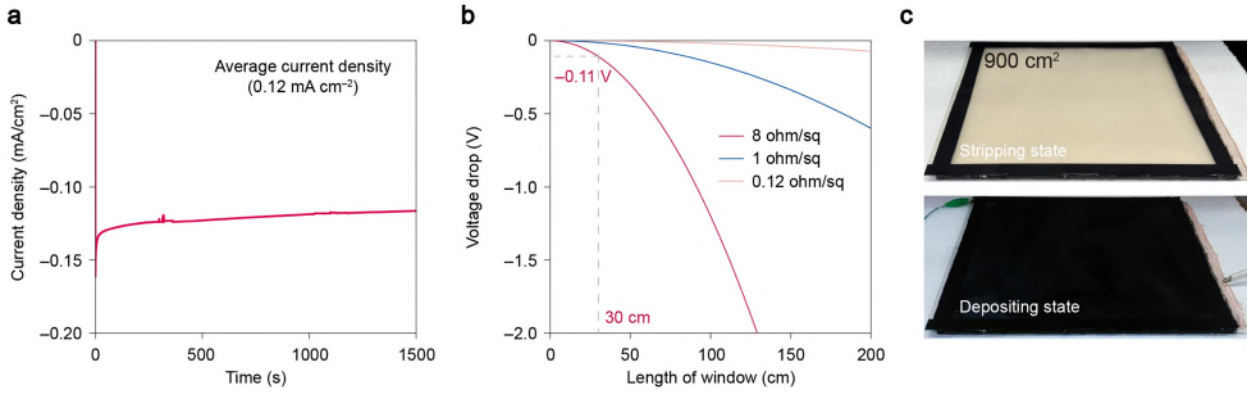

Figure R27. EC performance of large-area windows. **a**, Average depositing current density of a 900 cm^2 window. **b**, Voltage drops of the windows with different sheet resistances. **c**, A visual representation of a 900 cm^2 STDEC window with homogeneous deposition and coloration.

[Changes in revised manuscript]:

We have made two main changes in the revised manuscript and SI.

1. Page 8–9 of the revised manuscript.

We revised the sentence to emphasize the uniform deposition and coloration of the large-area STDEC window:

"*This decreased sheet resistance (e.g., 5 and 8 ohm/sq) helps to minimize the voltage drop from edge to center of our STDEC window (Supplementary Fig. 15), which promotes even deposition and tinting of the Cu–Bi films (Supplementary Figs. 16 and 17), and consequently protects against strong solar radiation in hot weather.*

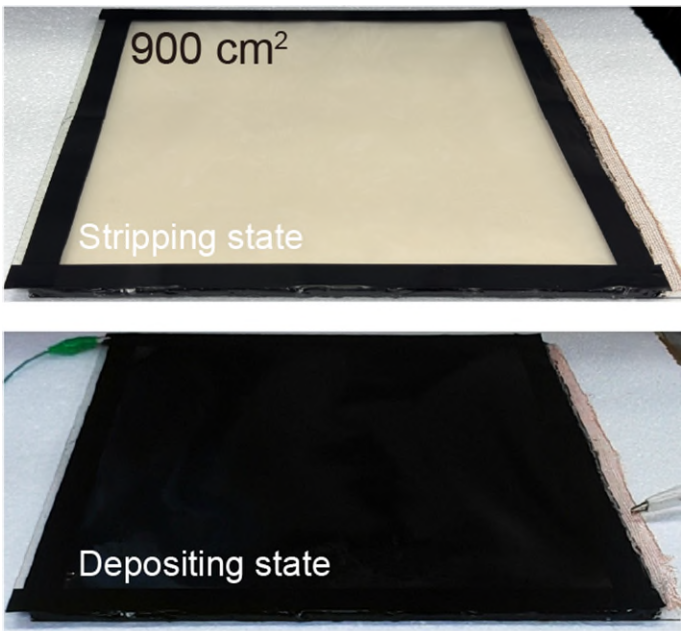

Supplementary Fig. 17: A visual representation of a 900 cm^2 STDEC window with homogeneous deposition and coloration."

2. Page 19 of the revised manuscript.

In the **Discussion** section, we have added a forward-looking perspective. Future work will explore metre-scale architectural STDEC windows for real-world applications:

"*Moreover, its commercial application calls for the metre-scale architectural windows, which can be addressed through device structural design with highly conductive and transparent electrodes*[54]*, patterned electrodes, or modular units, representing a critical direction for future research and technological development.*

References

54. Chen, X. et al. Highly conductive omnidirectionally stretchable 2D transparent copper mesh electrodes and applications in optoelectronic devices. Adv. Mater. Technol. ***8****, 2201406 (2023).*"

Response to Referee Reports for “Solar and Thermal Dual-Band Electrochromic Windows for Energy-Efficient Buildings”

We sincerely thank all reviewers for their timely review, constructive feedback, and positive assessment of our work.

Response to Reviewer 1

[General Comment]: Now, there are no concerns. I recommend to accept this paper.

[Response]: We sincerely thank Reviewer 1 for the positive feedback and recommendation to accept the paper.

Response to Reviewer 2

[General Comment]: I am impressed by both the quantity and the quality of the work carried out on the manuscript during the revision process. The authors addressed the extensive comments from all reviewers. Results are very solid and clearly presented. The overall quality of the paper has significantly improved. I recommend acceptance in its present form.

[Response]: We are truly grateful to Reviewer 2 for the positive feedback and recognition of our revisions. Your insightful suggestions have greatly improved the manuscript, and we are delighted that it now meets your expectations.